INTERNATIONAL JOURNAL FOR NUMERICAL METHODS IN ENGINEERING, VOL. 39, 951–985 (1996)

TWO-DIMENSIONAL ELASTODYNAMIC TRANSIENT ANALYSIS BY QL TIME-DOMAIN BEM FORMULATION

CHUNG-CHENG WANG*

Department of Civil Engineering, National Chiao Tung University, Hsinchu 30050, Taiwan

HUI-CHING WANG†

Department of Applied Mathematics, National Chung Hsing University, Taichung 40203, Taiwan

GIN-SHOW LIOU‡

Department of Civil Engineering, National Chiao Tung University, Hsinchu 30050, Taiwan

SUMMARY

A quadratic time-domain Boundary Element Method (BEM) for two-dimensional (2-D) elastodynamic transient wave analysis is presented. Emphasis is focused on developing time-domain fundamental convoluted kernels and methodology for quadratic temporal solution procedure which are never presented before. In the presented BEM method, the displacement temporal variation is assumed to be quadratic, the traction temporal variation is assumed to be linear (called QL method, a two-time-step piecewise continuity method), and the spatial variations are assumed to be quadratic variation. The QL method is compared with the LC method and the QC method by solving several example problems. Numerical study reveals that the QC and QL methods are more accurate and stable than the LC method, and the QL method is much better than the QC method for transient problems.

KEY WORDS: time-domain BEM; 2-D convoluted kernel; transient wave; quadratic temporal variation; elastodynamics

1. INTRODUCTION

Boundary Element Method (BEM) has recently become an important method in engineering analyses of linear elastodynamic problems, for example transient analysis and non-destructive testing, etc. Its popularity can be attributed primarily to the reduction of dimensionality of the problems, high accuracy of results and automatic consideration of the radiation conditions at infinity.[1] Compared to BEM in frequency or Laplace transformed domains, the time-domain BEM is still quite new and rarely touched, although it has been long acknowledged that the time-domain BEM is more attractive, especially for non-linear problems. Cruse and Rizzo[2] solved 2-D transient elastodynamic problems in the Laplace transformed domain by using BEM and a numerical inversion scheme to obtain time-domain solutions. After that, quite a few researchers solved transient problems using the transformed domain formulations.

* Graduate Student
† Associated Professor
‡ Professor

CCC 0029–5981/96/060951–35

Received 20 January 1995
Revised 5 July 1995

In the early 1980s, Niwa *et al.*[3] solved 2-D problems using 3-D transient kernels with the third spatial co-ordinate playing a role of time related variable. But Mansur[4] was the first to formulate a time-stepping algorithm using 2-D time-domain elastodynamic kernels. Later, Antes[5] also employed a similar formulation. Recently, Israil and Banerjee[6-8] implemented the numerical time-stepping technique and also gave a number of numerical solutions. In all these works, the temporal convolution integrals are evaluated analytically and the spatial integrations are carried out numerically at each time step. Wang and Takemiya[9] also obtained analytically both spatial and temporal integration for scalar wave by the Cagniard–De Hoop method.

In all the time-domain BEM methods mentioned above, the temporal variation of field variables is assumed to be either zeroth or first order (constant or linear) and piecewise continuous only in one time step. Some of previous works indicate that the time-domain BEM analysis combining linear approximation in displacement and constant approximation in traction field (called LC method, Israil and Banerjee[7] called it mixed variation) obtains better result than those by simply using linear variation (LL method) or constant variation (CC method). Besides these works, the quadratic temporal solution procedure (second-order, piecewise continuous in two time steps) is developed by the authors[10] for the first time. In the procedure, quadratic temporal variation for displacement and constant temporal variation for traction are adopted and spatial fields variations are assumed to be quadratic. Therefore, it is called QC method. As expected QC method gives better result than LL, CC and LC. Here the QL method is developed in the paper in which quadratic temporal variation for displacement and linear instead of constant temporal variation for traction are chosen, and spatial fields variations are also quadratic. Therefore, it is called QL method. The temporal integrations can be obtained analytically and the spatial integration is obtained using Gaussian quadrature method. The uniform subsegmentation technique is also used for the numerical integrations, since the kernels have singularities as well as jumps at the moving wave front.

As for wave fronts in which the divergent integral is treated in the sense of Cauchy Principal Value, the finite part of the integral is evaluated in this paper by using the method of rigid body translation, which is an indirect integration technique and can be found in most of BEM texts for elastostatics; e.g. Reference 11 or 12.

Several numerical examples are used to demonstrate the efficiency, effectiveness and numerical stability of the presented QL method. Some comparative studies are also made for QL method with QC and LC methods.

2. BEM INTEGRAL REPRESENTATION FORMULAE

Considering a domain V bounded by a surface S, the displacement $u_j(\xi, t)$ at a point ξ and at time t can be obtained by the dynamic reciprocal work theorem in an integral form as follows:

$$C_{ij}(\xi)u_j(\xi, t) = \int_S \{G_{ij}(\xi, \tau; \mathbf{x}, t) * t_j(\mathbf{x}, t) - F_{ij}(\xi, \tau; \mathbf{x}, t) * u_j(\mathbf{x}, t)\}\, \mathrm{d}S(\mathbf{x})$$

$$+ \rho \int_V G_{ij}(\xi, \tau; \mathbf{x}, t) * b_j(\mathbf{x}, t)\, \mathrm{d}V(\mathbf{x})$$

$$+ \rho \int_V \{G_{ij}(\xi, \tau; \mathbf{x}, t)\dot{u}_j(\mathbf{x}, 0) + \dot{G}_{ij}(\xi, \tau; \mathbf{x}, t)u_j(\mathbf{x}, 0)\}\, \mathrm{d}V(\mathbf{x}) \qquad (1)$$

In the above equation, $C_{ij}(\xi)$ is the well-known discontinuity term which is dependent on local geometry. And $*$ stands for the Reimann convolution integral, $t_j(\mathbf{x}, t)$ is the traction vector, b_j is the jth component of the body force, the overdots indicate the time derivative. The terms $G_{ij}(\xi, \tau; \mathbf{x}, t)$ and $F_{ij}(\xi, \tau; \mathbf{x}, t)$ are the fundamental solutions and represent, respectively, the displacements and tractions at the field point $\mathbf{x}$ and at time t due to a unit point force applied at the source point ξ and a preceding time τ.

The governing equation (1) for elastodynamic problems represents an exact formulation involving integrations over the surface and the volume as well as the time history. It is also of interest to note that equation (1) is an implicit time-domain formulation, since the displacements at time t are calculated by taking account of the history of surface tractions and the history of displacements up to the time t.

2.1. *Fundamental Solution*

The desired 2-D kernel, is written for completeness as follows:

$$G_{ij}(\xi, \tau; \mathbf{x}, t) = \frac{1}{2\pi\rho}\left\{\frac{H(c_1t' - r)}{c_1}\left[\frac{2\left(\frac{c_1t'}{r}\right)^2 - 1}{\sqrt{\left(\frac{c_1t'}{r}\right)^2 - 1}}\left(\frac{r_{,i}r_{,j}}{r}\right) - \frac{\delta_{ij}}{r}\sqrt{\left(\frac{c_1t'}{r}\right)^2 - 1}\right]\right.$$

$$\left. + \frac{H(c_2t' - r)}{c_2}\left[\frac{2\left(\frac{c_2t'}{r}\right)^2 - 1}{\sqrt{\left(\frac{c_2t'}{r}\right)^2 - 1}}\left(\frac{r_{,i}r_{,j}}{r}\right) + \frac{\delta_{ij}}{r}\frac{\left(\frac{c_2t'}{r}\right)^2}{\sqrt{\left(\frac{c_2t'}{r}\right)^2 - 1}}\right]\right\} \tag{2}$$

where H is the Heaviside function and $t' = t - \tau$ is the retarded time; r denotes the distance $|\mathbf{x} - \xi|$; c_1 is the velocity of dilatational wave defined by $c_1^2 = (\lambda + 2\mu)/\rho$ and c_2 is the velocity of shear wave defined by $c_2^2 = \mu/\rho$, λ and μ are the Lamé's constants and ρ is the mass density of the material, and the inferior commas indicate space derivatives. The details of derivation of equation (2) can be found in the text by Eringen and Suhubi,[13] and the form was written by Israil and Banerjee.[6,8]. The F_{ij} kernel (the traction kernel) can be obtained using the strain–displacement relationship and the constitutive equations (Hooke's law) as

$$F_{ij}(\xi, \tau; \mathbf{x}, t) = \frac{\mu}{2\pi\rho r}\left\{\frac{1}{c_1}H\left(\frac{c_1t'}{r} - 1\right)\left[\frac{1}{\left\{\left(\frac{c_1t'}{r}\right)^2 - 1\right\}^{3/2}}\left(\frac{A_{ij}^1}{r}\right) + \frac{2\left(\frac{c_1t'}{r}\right)^2 - 1}{\sqrt{\left(\frac{c_1t'}{r}\right)^2 - 1}}\left(\frac{2A_{ij}^2}{r}\right)\right]\right.$$

$$\left. - \frac{\delta(c_1t' - r)}{c_1}\left[A_{ij}^1\frac{2\left(\frac{c_1t'}{r}\right)^2 - 1}{\sqrt{\left(\frac{c_1t'}{r}\right)^2 - 1}} - B_{ij}^2\sqrt{\left(\frac{c_1t'}{r}\right)^2 - 1}\right]\right.$$

$$-\frac{1}{c_2}H\left(\frac{c_2t'}{r}-1\right)\left[\frac{1}{\left\{\left(\frac{c_2t'}{r}\right)^2-1\right\}^{3/2}}\left(\frac{A_{ij}^3}{r}\right)+\frac{2\left(\frac{c_2t'}{r}\right)^2-1}{\sqrt{\left(\frac{c_2t'}{r}\right)^2-1}}\left(\frac{2A_{ij}^2}{r}\right)\right]$$

$$+\frac{\delta(c_2t'-r)}{c_2}\left[A_{ij}^1\frac{2\left(\frac{c_2t'}{r}\right)^2-1}{\sqrt{\left(\frac{c_2t'}{r}\right)^2-1}}-B_{ij}^2\frac{\left(\frac{c_2t'}{r}\right)^2}{\sqrt{\left(\frac{c_2t'}{r}\right)^2-1}}\right]\Bigg\} \tag{3}$$

where

$$A_{ij}^1=\left(\frac{\lambda}{\mu}\right)n_jr_{,i}+2r_{,i}r_{,j}\frac{\partial r}{\partial n} \tag{4}$$

$$A_{ij}^2=n_ir_{,j}+n_jr_{,i}+\frac{\partial r}{\partial n}(\delta_{ij}-4r_{,i}r_{,j}) \tag{5}$$

$$A_{ij}^3=\frac{\partial r}{\partial n}(2r_{,i}r_{,j}-\delta_{ij})-n_ir_{,j} \tag{6}$$

$$B_{ij}^2=\frac{\lambda}{\mu}n_jr_{,i}+r_{,j}n_i+\delta_{ij}\frac{\partial r}{\partial n} \tag{7}$$

In equations (4)–(7), n_i denotes the unit normal vector to S. The above expressions for the 2-D transient F_{ij}-kernel are the most explicit and simplest available so far. Also, one should note that the terms involving the delta function $\delta(c_it'-r)$ represent the waves front contribution. After spatial integration, these terms make no contribution.

2.2 *Temporal integration*

For the numerical implementation of equation (1), discretizations in both time and space are required. The time integrations can be performed analytically while the spatial integrations are treated numerically. The salient features of the temporal integrations will be presented in what follows.

In evaluating the convoluted $G_{ij}*t_j$ and $F_{ij}*u_j$ kernels, the computational effort can be greatly reduced by making use of the time-translation and causality property of the kernels. That is, at each time step, only the effect of the current time interval is needed to be evaluated.

The time span of interest is discretized into N time steps with a duration Δt for one time step. And define $t_n=n\,\Delta t$ for $n=1,2,\ldots,N$. The temporal variations of the functions are described in the following.

2.2.1 Quadratic temporal interpolation functions. The field variables are assumed to vary quadratically during a two time step and can be expressed as

$$f_i(\mathbf{x},\tau)=M_{\mathrm{QF}}(\tau)f_i^n(\mathbf{x})+M_{\mathrm{QM}}(\tau)f_i^{n-1}(\mathbf{x})+M_{\mathrm{QB}}(\tau)f_i^{n-2}(\mathbf{x}) \tag{8}$$

where $f_i^n(\mathbf{x})$ stands for tractions or displacements at time step n and $M_{QF}(\tau)$, $M_{QM}(\tau)$ and $M_{QB}(\tau)$ are quadratic temporal interpolation functions as shown in Figure 1(a) and given by:

$$M_{QF}(\tau) = \frac{1}{2}\left(\frac{\tau - t_{n-2}}{\Delta t}\right)^2 - \frac{1}{2}\left(\frac{\tau - t_{n-2}}{\Delta t}\right) \tag{9}$$

$$M_{QM}(\tau) = -\left(\frac{\tau - t_{n-2}}{\Delta t}\right)^2 + 2\left(\frac{\tau - t_{n-2}}{\Delta t}\right) \tag{10}$$

$$M_{QB}(\tau) = \frac{1}{2}\left(\frac{\tau - t_{n-2}}{\Delta t}\right)^2 - \frac{3}{2}\left(\frac{\tau - t_{n-2}}{\Delta t}\right) + 1 \tag{11}$$

in which $t_{n-2} \leqslant \tau \leqslant t_n$, the subscripts QF, QM and QB are referred, respectively, to the forward, midpoint and backward temporal nodes in two time steps ($2\,\Delta t$).

2.2.2. Linear temporal interpolation functions. The field variables are approximated by using linear interpolation functions during a time step and can be expressed as follows:

$$f_i(\mathbf{x}, \tau) = M_{LF}(\tau) f_i^n(\mathbf{x}) + M_{LB}(\tau) f_i^{n-1}(\mathbf{x}) \tag{12}$$

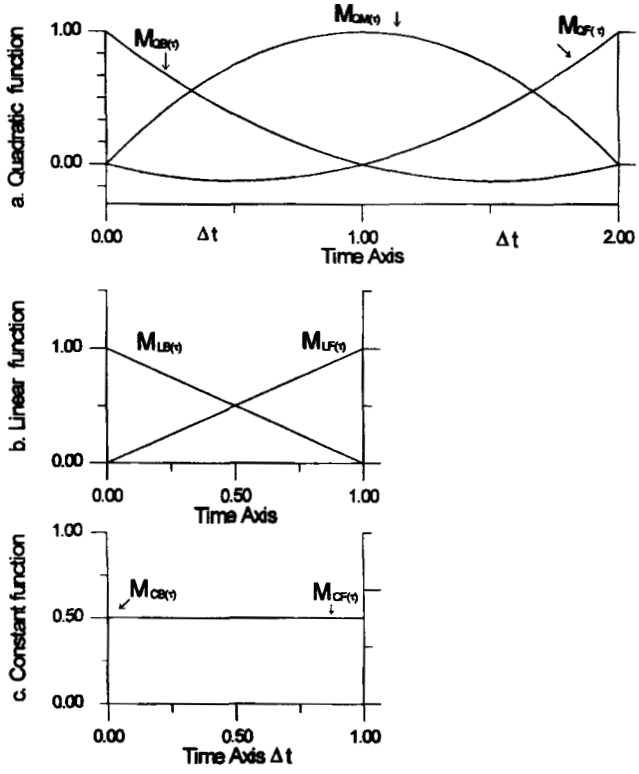

Figure 1. Temporal interpolation functions, (a) quadratic, (b) linear, (c) constant

where $M_{LF}(\tau)$ and $M_{LB}(\tau)$ are linear temporal interpolation functions given by

$$M_{LF}(\tau) = \frac{\tau - t_{n-1}}{\Delta t}, \quad M_{LB}(\tau) = \frac{t_n - \tau}{\Delta t}; \quad t_{n-1} \leqslant \tau \leqslant t_n \tag{13}$$

in which the subscripts LF and LB are referred to the forward and backward linear temporal nodes, respectively, in a time step as shown in Figure 1(b). More precisely, it is important to distinguish linear variation of a linear step from linear variation of a quadratic step.

2.2.3. Constant temporal interpolation functions. If a constant variation is assumed, then the field variables can be expressed as follows:

$$f_i(\mathbf{x}, \tau) = M_{CF}(\tau) f_i^n(\mathbf{x}) + M_{CB}(\tau) f_i^{n-1}(\mathbf{x}) \tag{14}$$

where $M_{CF}(\tau)$ and $M_{CB}(\tau)$ are constant temporal interpolation functions given by

$$M_{CF}(\tau) = \tfrac{1}{2}, \quad M_{CB}(\tau) = \tfrac{1}{2}; \quad t_{n-1} \leqslant \tau \leqslant t_n \tag{15}$$

in which the subscripts CF and CB are referred to the forward and backward constant temporal nodes, respectively, in a time step as shown in Figure 1(c).

2.3. *Quadratic solution procedure*

For elastodynamic problems with initial rest conditions and in the absence of the body force, only the surface integral in equation (1) remains. Thus, time-domain boundary element equations can be expressed as follows:

$$\begin{aligned} C_{ij}(\xi) u_j^N(\xi) - \int_{(N-2)\Delta t}^{N\Delta t} \int_S ([G_{ij} t_j(\mathbf{x}, \tau) - F_{ij} u_j(\mathbf{x}, \tau)]) \, dS(\mathbf{x}) \, d\tau \\ = \int_0^{(N-2)\Delta t} \int_S ([G_{ij} t_j(\mathbf{x}, \tau) - F_{ij} u_j(\mathbf{x}, \tau)]) \, dS(\mathbf{x}) \, d\tau \\ = R^N \end{aligned} \tag{16}$$

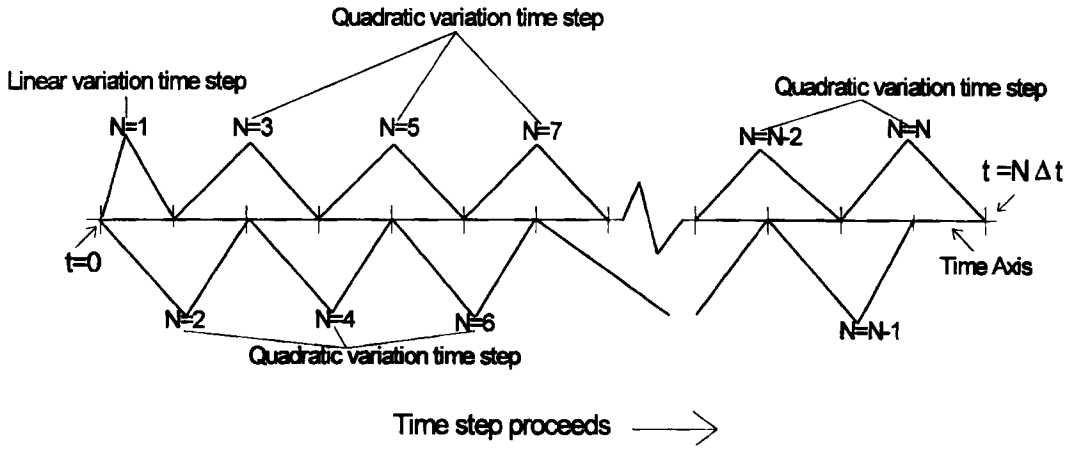

Figure 2. Quadratic temporal solution procedure

in which R^N represents the effect of past dynamic history on the current time node. The reason why two time steps are used in equation (16) is that the analytic integrations for quadratic temporal function representing boundary displacement field can be developed. However, one should note that only a single time step is chosen in this paper for the first time step $N = 1$. In other words, the first time step is the linear or constant step. After the first time step, fully

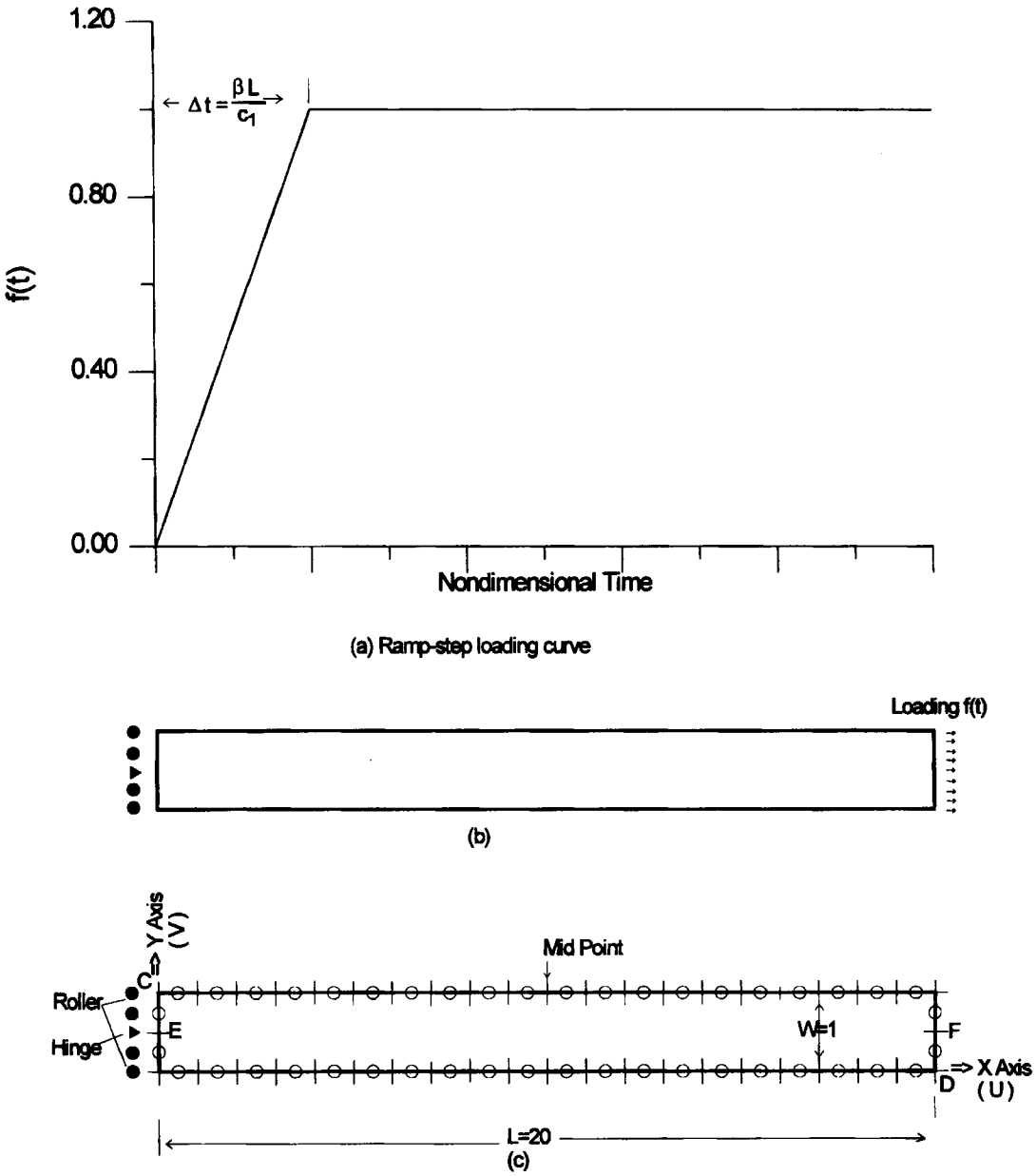

Figure 3. Boundary element discretization of a cantilever bar, $L/W = 20$, 88 nodes with 44 quadratic elements

quadratic temporal solution procedure can then be established as shown in Figure 2. Now, the solution procedure will be dependent upon N is even or odd. The developed methodology for quadratic temporal solution procedure is presented as follows.

If N is even, let $N = 2K$. With the quadratic variation of temporal functions described in equation (8), equation (16) becomes the following form:

$$C_{ij}(\xi)u_j^{2K}(\xi) = \sum_{n=1}^{K} \int_S ([G_{QFij}^{2K-2n+2} + G_{QBij}^{2K-2n}]t_j^{2n}(\mathbf{x}) + [G_{QMij}^{2K-2n+2}]t_j^{2n-1}(\mathbf{x}) - [F_{QFij}^{2K-2n+2} + F_{QBij}^{2K-2n}]t_j^{2n}(\mathbf{x}) + [F_{QMij}^{2K-2n+2}]u_j^{2n-1}(\mathbf{x}))\,dS(\mathbf{x}) \tag{17}$$

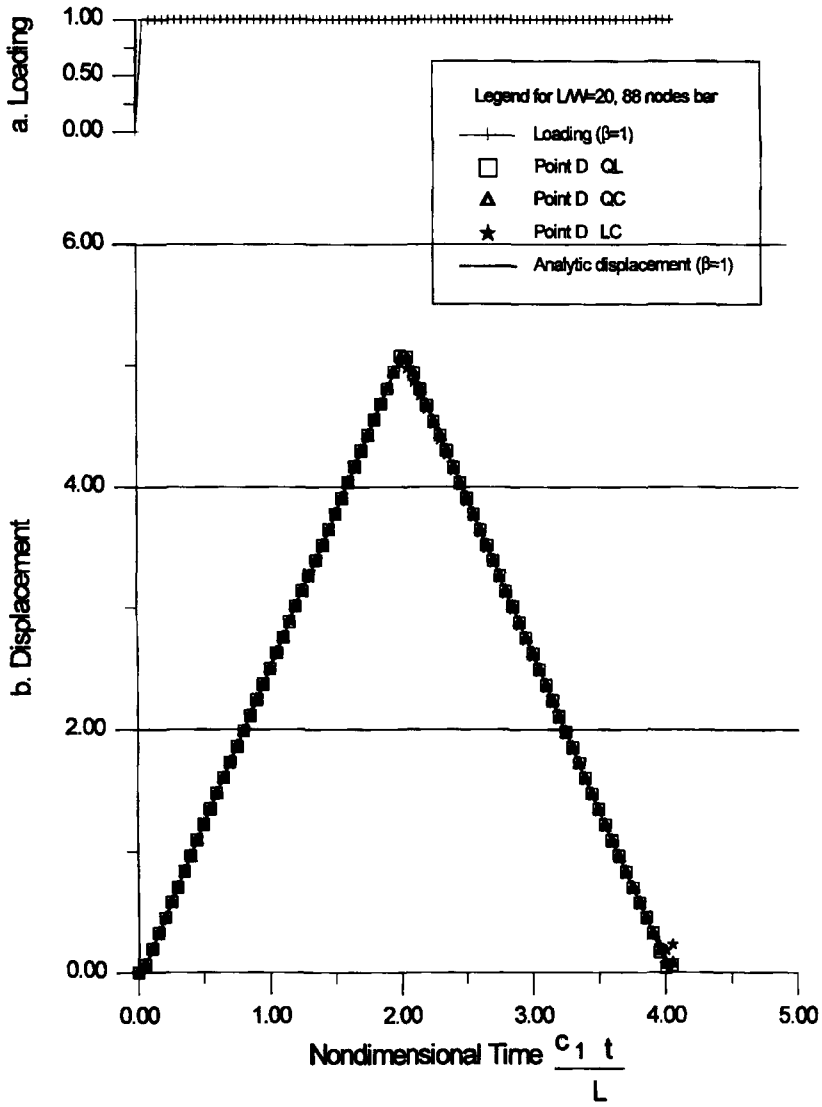

Figure 4. Comparison of the QL with the LC and QC method for time step $\beta = 1{\cdot}0$

In equation (17), one should note that every piecewise continuous function is a two-time-step function. In addition, the initial tractions are assumed zero everywhere at boundary surface. For a Heaviside loading with non-zero initial value, a term of $G^{2K}_{QBij}t^0_j$ in equation (17) is neglected.

If N is odd, let $N = 2K + 1$. Equation (1) similarly takes the form:

$$C_{ij}(\xi)u_j^{2K+1}(\xi) = \sum_{n=1}^{K}\int_S ([G_{QFij}^{2K-2n+2} + G_{QBij}^{2K-2n}]t_j^{2n+1}(\mathbf{x}) + [G_{QMij}^{2K-2n+2}]t_j^{2n}(\mathbf{x}) - [F_{QFij}^{2K-2n+2} + F_{QBij}^{2K-2n}]t_j^{2n+1}(\mathbf{x}) + [F_{QMij}^{2K-2n+2}]u_j^{2n}(\mathbf{x}))\,dS(\mathbf{x}) + \int_S ([G_{LFij}^{2K+1} + G_{QBij}^{2K}]t_j^1(\mathbf{x}) - [F_{LFij}^{2K+1} + F_{QBij}^{2K}]u_j^1(\mathbf{x}))\,dS(\mathbf{x}) \quad (18)$$

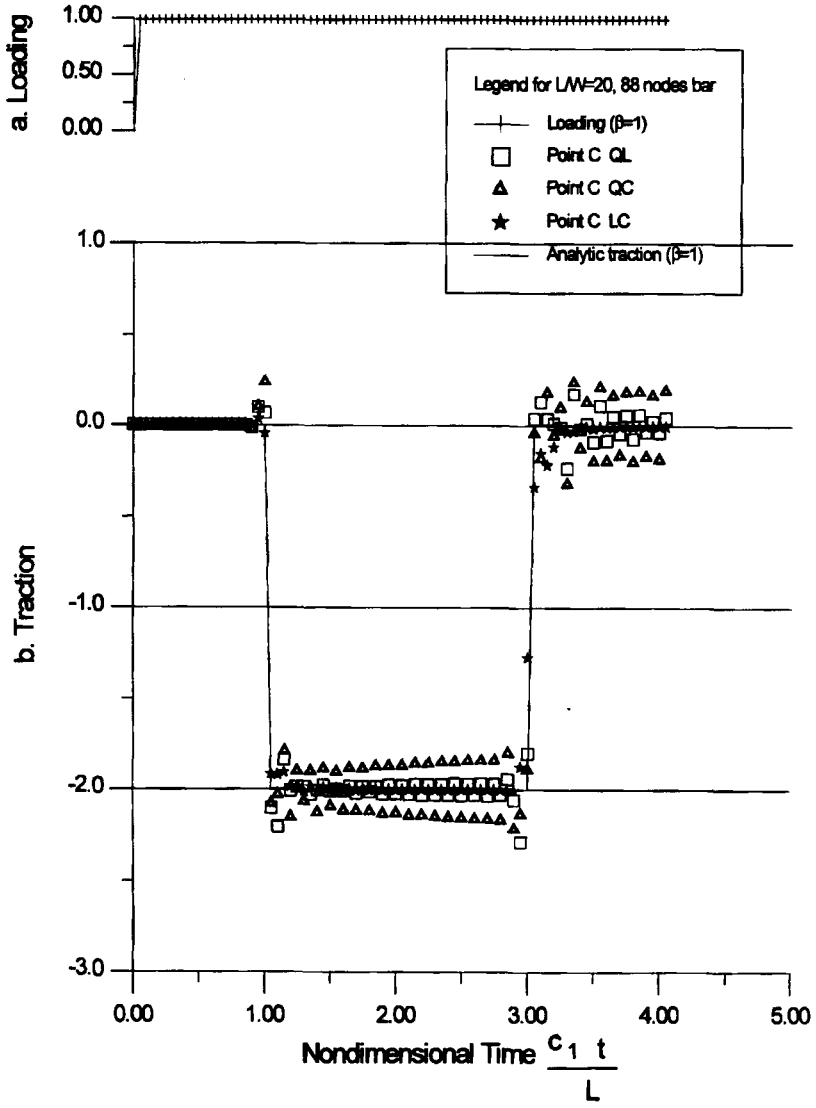

Figure 5. Comparison of the QL with the LC and QC method for time step $\beta = 1{\cdot}0$

In the above two equations, $[G_{QFij}^{N-2n+2} + G_{QBij}^{N-2n}]$, $[F_{QFij}^{N-2n+2} + F_{QBij}^{N-2n}]$, $[G_{QMij}^{2K-2n+2}]$ and $[F_{QMij}^{2K-2n+2}]$ are the quadratic convoluted combined kernels. The forward temporal point (QF) array and the backward temporal point (QB) array can be merged into one array as $[F_{QFij}^{N-2n+2} + F_{QBij}^{N-2n}]$ shows with the benefit of cancelling of strong singularity for $N > 2$. In equation (18), one should also note that only the first piecewise continuous function is one-time-step function and the other piecewise functions are two-time-step functions. The last term in equation (18) represents the first-time-step effect which includes parts of linear variation contribution and parts of quadratic variation contribution. Moreover, the fully quadratic convoluted combined kernels of equation (18) apparently equal that of equation (17).

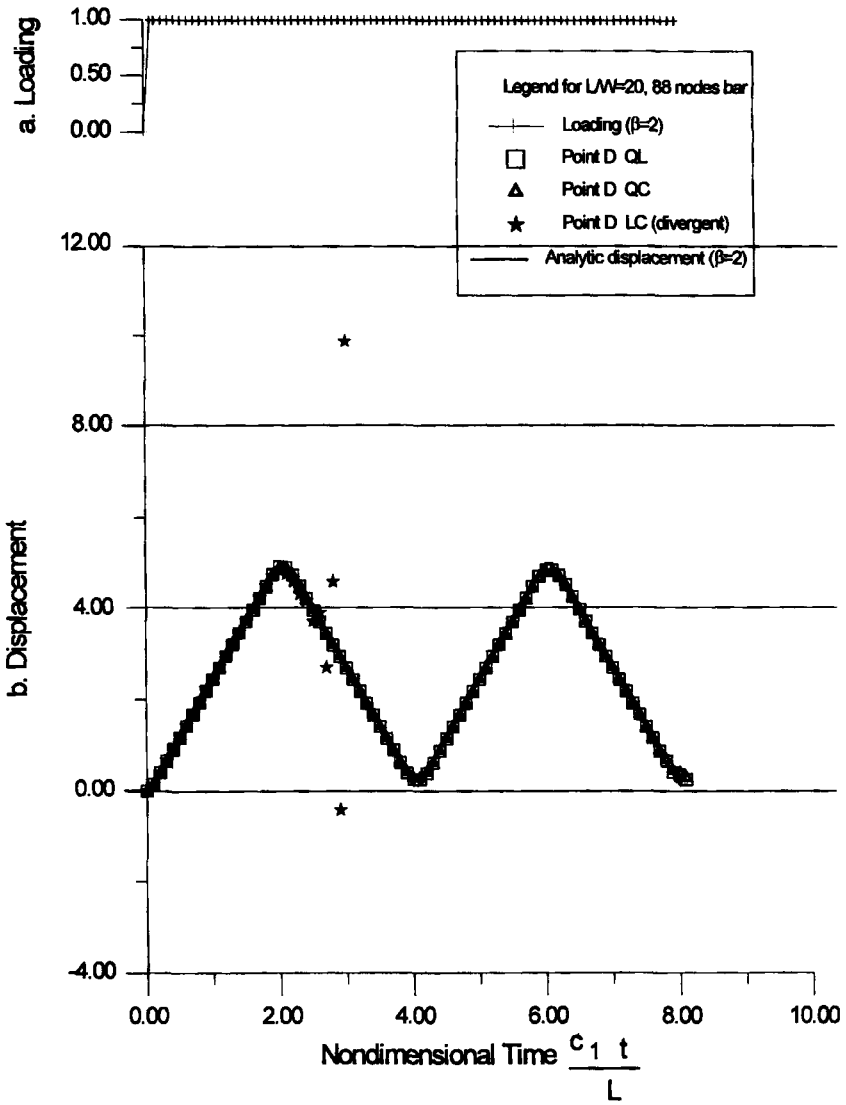

Figure 6. Comparison of the QL with the LC and QC method for time step $\beta = 2{\cdot}0$

Quadratic convolution combined traction kernels in equations (17) and (18) are defined as follows:

$$[F_{\mathrm{QF}ij}^{2K-2n+2} + F_{\mathrm{QB}ij}^{2K-2n}] \equiv \int_{(2n-2)\,\Delta t}^{2n\,\Delta t} F_{ij}(\xi, \tau; \mathbf{x}, 2K\,\Delta t) M_{\mathrm{QF}}(\tau)\,\mathrm{d}\tau + \int_{2n\,\Delta t}^{(2n+2)\,\Delta t} F_{ij}(\xi, \tau; \mathbf{x}, 2K\,\Delta t) M_{\mathrm{QB}}(\tau)\,\mathrm{d}\tau \tag{19}$$

and

$$[F_{\mathrm{QM}ij}^{2K-2n+2}] \equiv \int_{(2n-2)\,\Delta t}^{2n\,\Delta t} F_{ij}(\xi, \tau; \mathbf{x}, 2K\,\Delta t) M_{\mathrm{QM}}(\tau)\,\mathrm{d}\tau \tag{20}$$

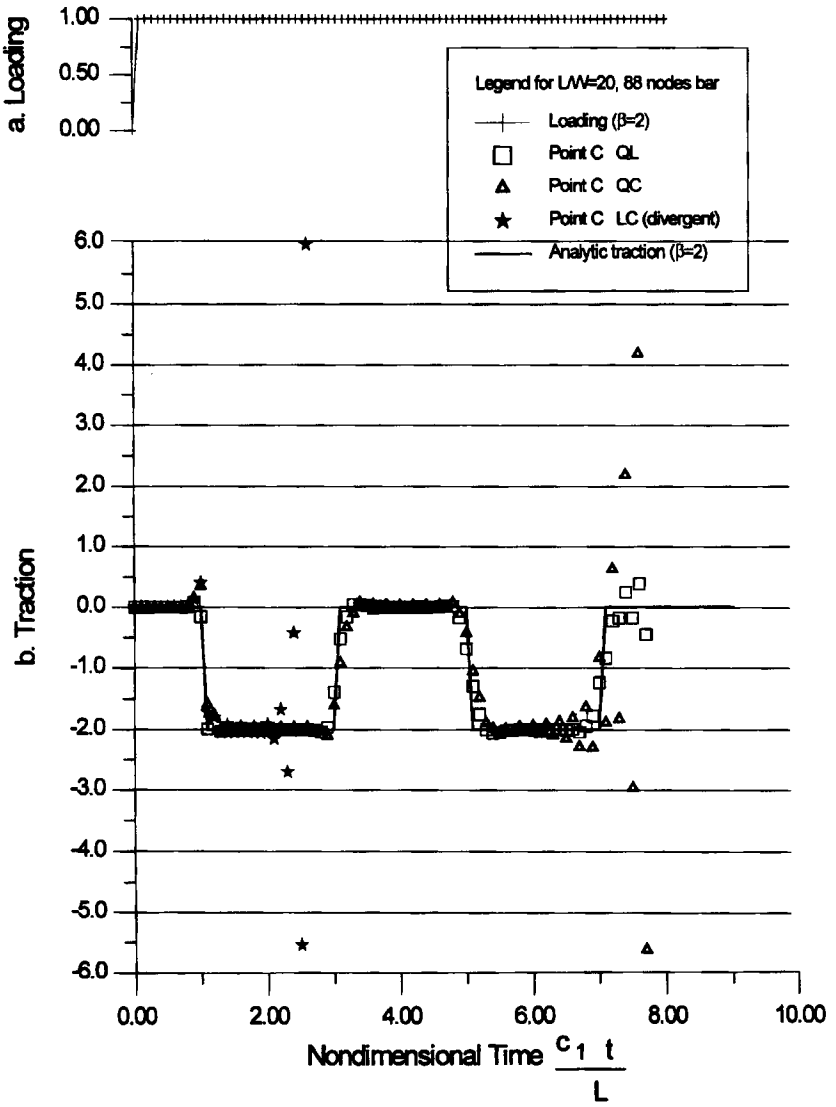

Figure 7. Comparison of the QL with the LC and QC method for time step $\beta = 2{\cdot}0$

in which F_{ij} is the fundamental solution of traction in equation (3), M_{QF}, M_{QM} and M_{QB} are quadratic temporal interpolation functions defined in equations (9)–(11). The quadratic convolution combined displacement kernels and the linear convolution combined kernels can be similarly obtained as, for example

$$[G_{LFij}^{N-n+1} + G_{LBij}^{N-n}] \equiv \int_{(n-1)\Delta t}^{n\Delta t} G_{ij}(\xi, \tau; \mathbf{x}, N\Delta t) M_{LF}(\tau)\, d\tau + \int_{n\Delta t}^{(n+1)\Delta t} G_{ij}(\xi, \tau; \mathbf{x}, N\Delta t) M_{LB}(\tau)\, d\tau \tag{21}$$

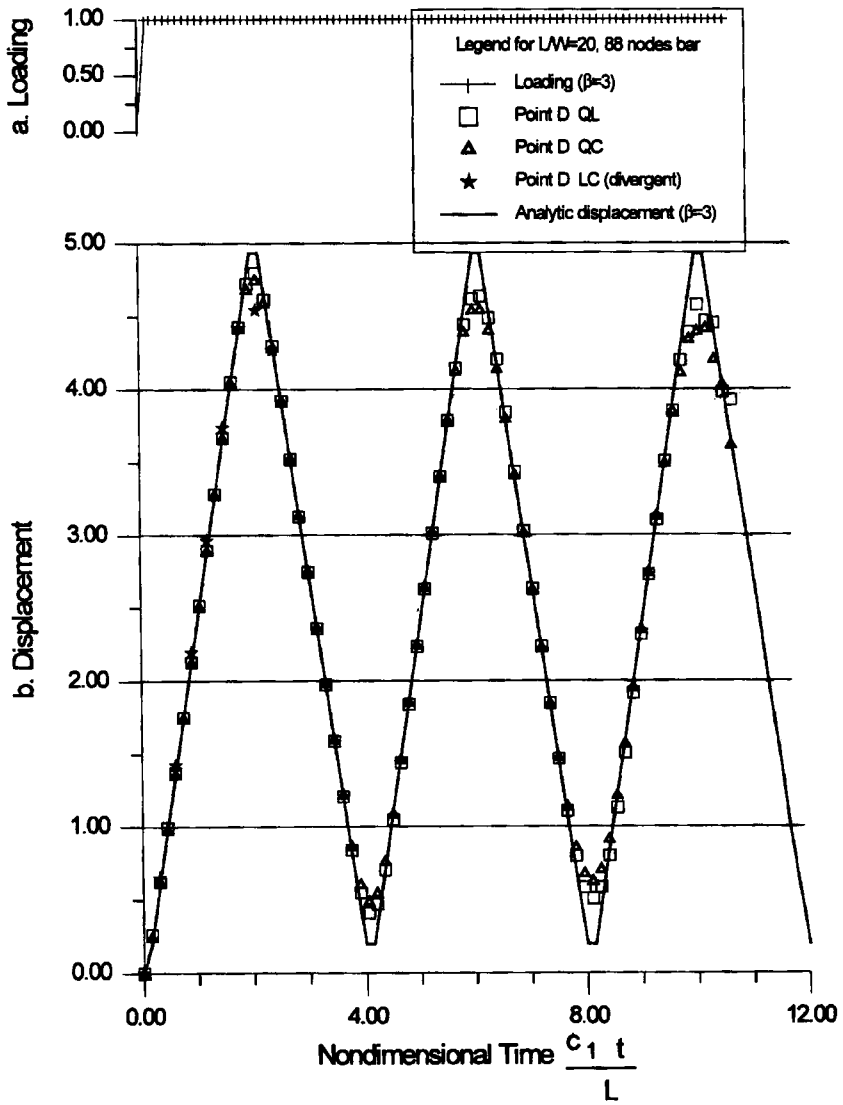

Figure 8. Comparison of the QL with the LC and QC methods for time step $\beta = 3{\cdot}0$

However, the convoluted $F_{ij} * u_j$ kernels contain terms that sometimes cause difficulty[7] in numerical integration especially for a mesh with widely varying element lengths. But, after convoluted kernels are combined as demonstrated in equations (17) and (18), those strong singular terms cancel each other and result in well-behaved functions for $N > 2$. And only at $N = 1$ (for linear variation time step) or $N = 2$ (for quadratic variation time step) strong singularity of $O(\frac{1}{r})$ occurs at wave fronts, which can be dealt with the well-known rigid body method[7] or the finite part method. Furthermore, the combined kernels form in equations (17) and (18) can save computer memory space by merging two arrays into one array.

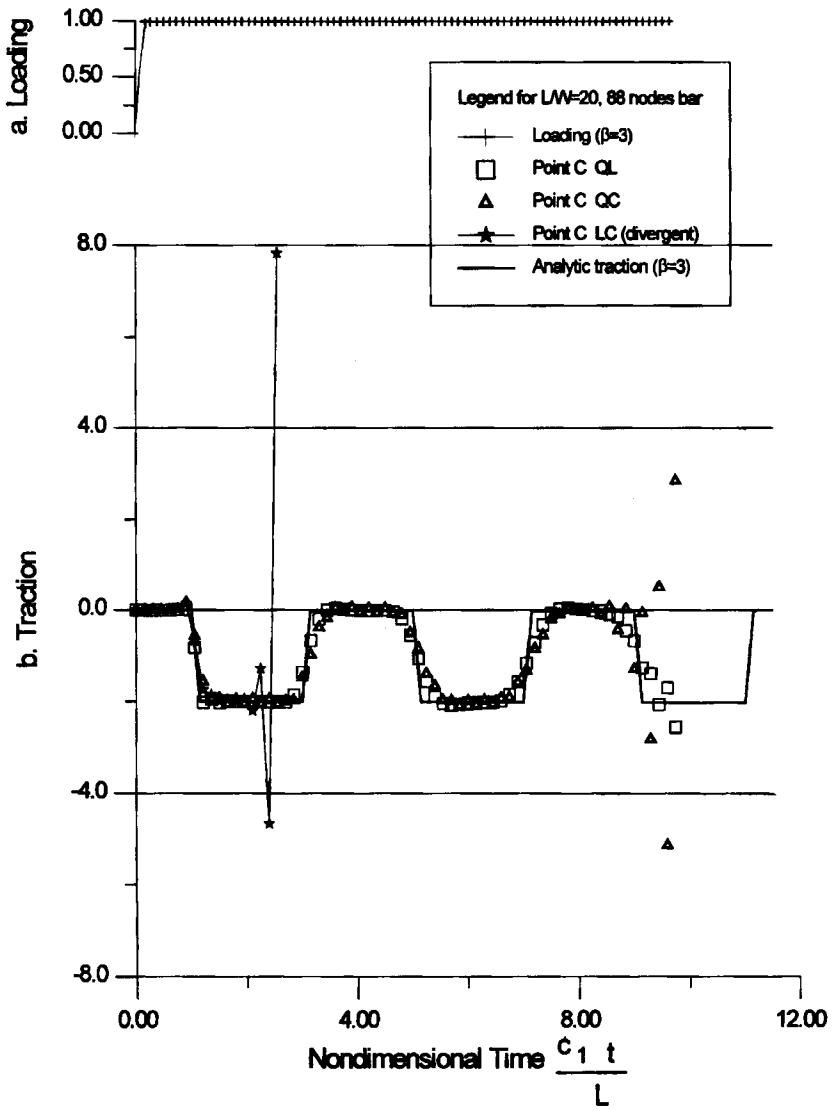

Figure 9. Comparison of the QL with the LC and QC method for time step $\beta = 3{\cdot}0$

2.3.1. QL mixed method solution procedure. The mixed solution procedure model is developed to combine different temporal displacement variations and traction variations. From the constitutive relationship, the stresses are the spatial derivative of displacements. This implies that it may be reasonable to employ the temporal interpolation function for displacement one order higher than that for traction.[9] The mixed variation procedure can similarly be obtained as quadratic variation procedure through simple manipulations. One can obtain the equivalent linear traction convoluted displacement combined kernels for $n = 1$ only, due to time translation property, as follows:

$$[G^N_{\mathrm{qLF}ij} + G^{N-2}_{\mathrm{qLB}ij}] \Rightarrow [G^N_{\mathrm{QF}ij} + G^{N-2}_{\mathrm{QB}ij}] \Leftarrow [G^{N-1}_{\mathrm{lLF}ij} + G^{N-2}_{\mathrm{lLB}ij}] \equiv [G^{N-1}_{\mathrm{LF}ij} + G^{N-2}_{\mathrm{LB}ij}] \tag{22}$$

$$[G^N_{\mathrm{qLM}ij}] \Rightarrow [G^N_{\mathrm{QM}ij}] \Leftarrow [G^N_{\mathrm{lLF}ij} + G^{N-1}_{\mathrm{lLB}ij}] \equiv [G^N_{\mathrm{LF}ij} + G^{N-1}_{\mathrm{LB}ij}] \tag{23}$$

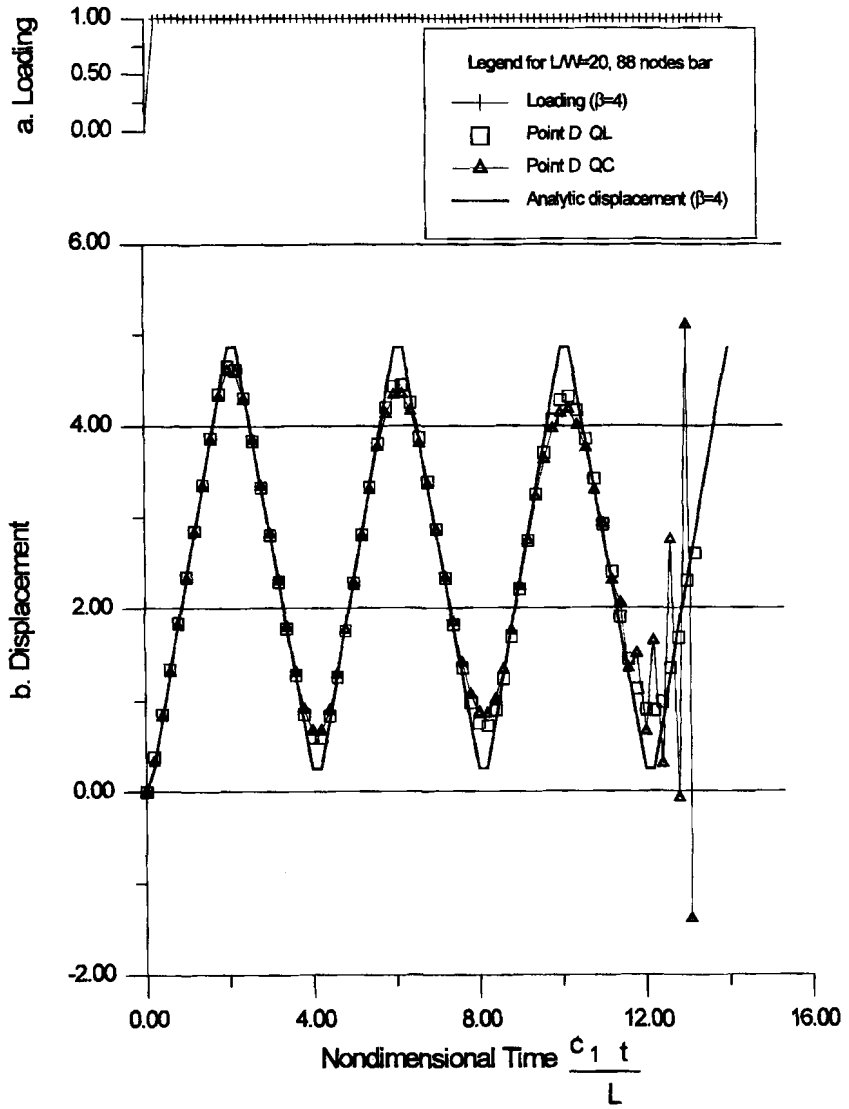

Figure 10. Comparison of the QL with the QC method for time step $\beta = 4{\cdot}0$

where the subscripts qLM, qLF and qLB are linear temporal variation for equivalent quadratic time step's mid-point, forward and backward temporal nodes, respectively. And the subscripts lLF and lLB are linear temporal point of linear time step's forward and backward nodes, respectively. It is worth to note that the analytical integral of linear variation for traction over quadratic time step should break into two pieces of linear time step in order to maintain the accuracy. The linearity of two time steps for traction convolution kernels is similar to that of one time step. The linear convoluted displacement kernels with quadratic temporal step are expressed as equivalent linear convoluted displacement kernels with linear temporal step and they are given by equations (27)–(29) of Appendix I. And the quadratic convolution traction combined kernels with quadratic temporal step are defined by equations (30)–(32) of Appendix I.

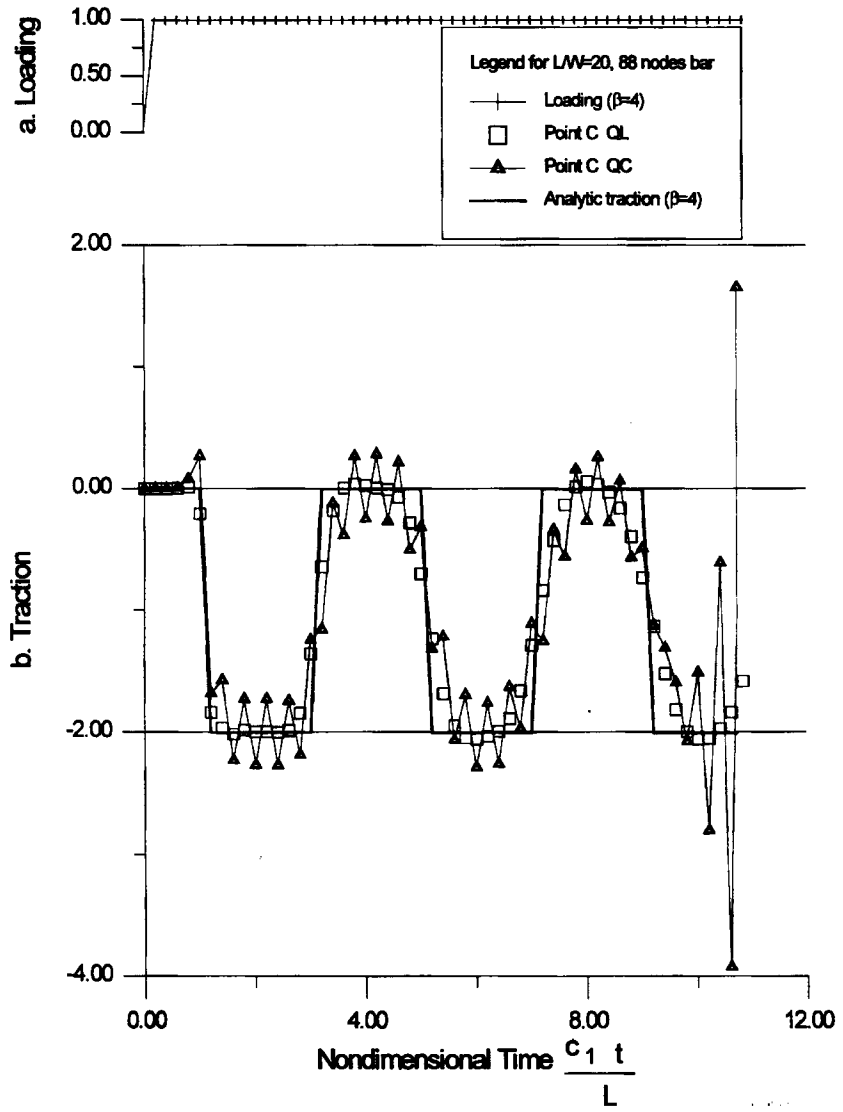

Figure 11. Comparison of the QL with the QC method for time step $\beta = 4{\cdot}0$

The QL method solution procedure can be similarly obtained by using equations (22), (23) and substituting linear-and-quadratic variation of $[G_{\mathrm{LF}ij}^{2K+1} + G_{\mathrm{QB}ij}^{2K}]$ with linear-and-linear variation of $[G_{\mathrm{LF}ij}^{2K+1} + G_{\mathrm{LB}ij}^{2K}]$ into equations (17) and (18).

For the LC method (linear temporal variation for displacement and constant temporal variation for traction) the solution procedure can be expressed as follows:

$$C_{ij}(\xi)u_j^N(\xi) = \sum_{n=1}^{N} \int_S ([G_{\mathrm{CF}ij}^{N-n+1} + G_{\mathrm{CB}ij}^{N-n}]t_j^n(\mathbf{x}) - [F_{\mathrm{LF}ij}^{N-n+1} + F_{\mathrm{LB}ij}^{N-n}]u_j^n(\mathbf{x})\,\mathrm{d}S(\mathbf{x}) \tag{24}$$

where the subscripts LF and LB are the forward and backward temporal nodes of linear time step as depicted in Figure 1(b), respectively.

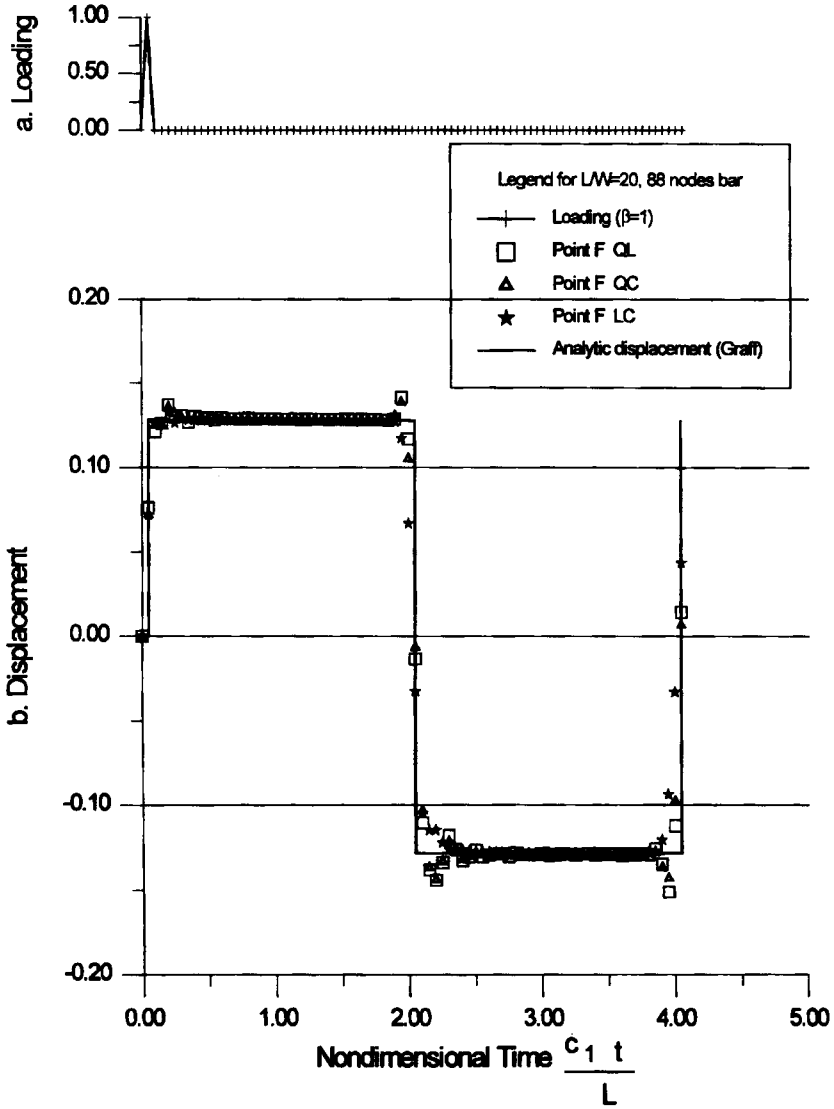

Figure 12. Comparison of the QL with the LC and QC method for time step $\beta = 1{\cdot}0$

In the above equations, the solution procedures represent an exact formulation of integrations over the surface, if the assumption of field variables variation were made.

3. NUMERICAL RESULTS

The following examples are presented to demonstrate the capability of the proposed QL method. The boundary geometry is modelled with continuous isoparametric quadratic elements. The surface traction components on both elements attached to the corner node can be different.

In general, the spatial variation of the convoluted kernels is an Heaviside logarithmic or square root decay function and hence uniform subsegmentation techniques are used for accurate

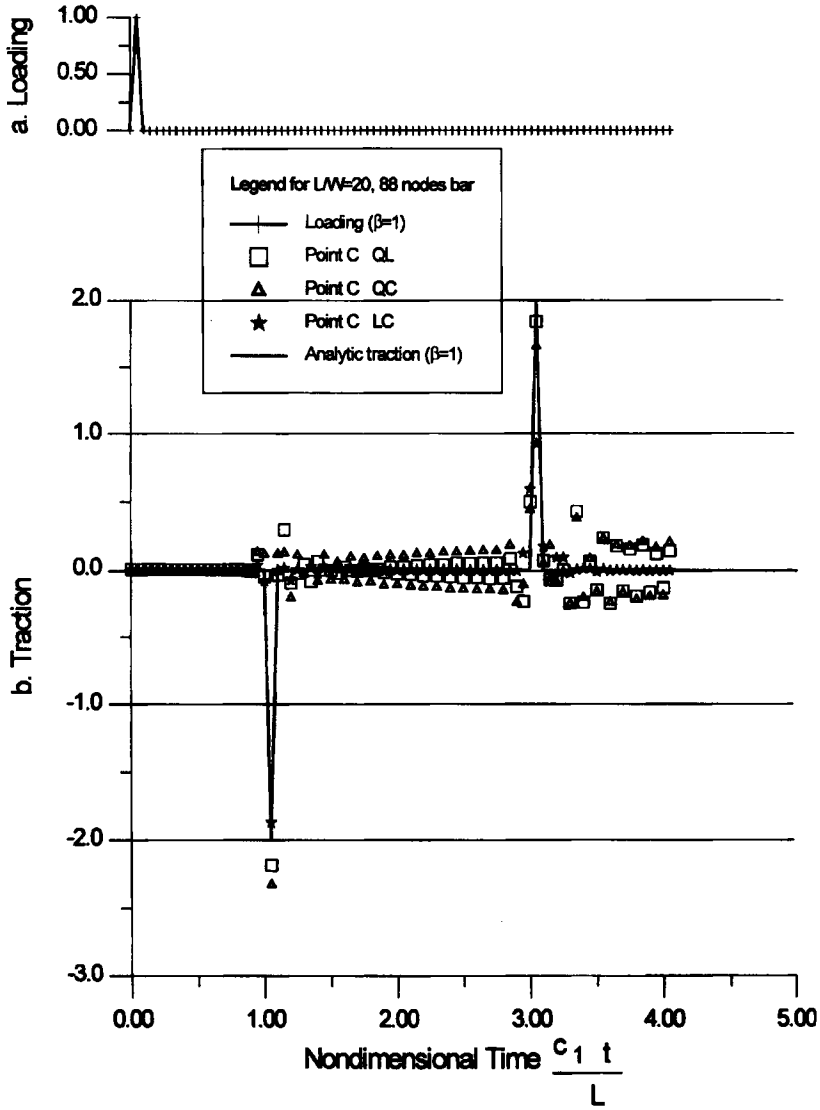

Figure 13. Comparison of the QL with the LC and QC method for time step $\beta = 1{\cdot}0$

evaluation of the spatial integrals. 12×32 and 8×10 in which the first number indicates the number of subsegments and the second number indicates the number of Gauss points for one subsegment, are selected for evaluating of the singular and non-singular time step, respectively, for the three (LC, QC and QL) methods used in the paper. In the following examples, the same spatial discretization and Gauss points are used in LC, QC and QL methods for comparison.

The non-dimensionalized time step β is defined as

$$\beta \equiv \frac{c_1 \Delta t}{l} \tag{25}$$

where l is the quadratic element length, Δt is the time step used and c_1 is the compressional wave velocity. Since a larger β means less computing time, the numerical investigation about β is also

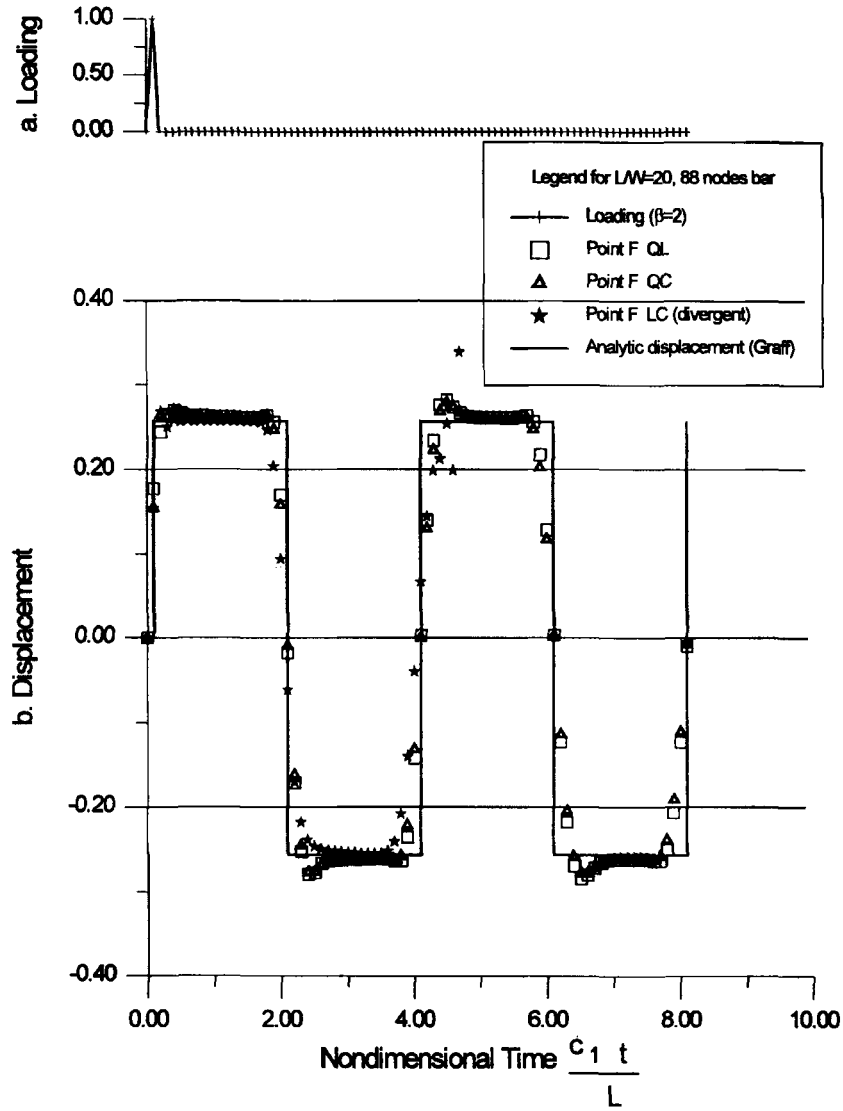

Figure 14. Comparison of the QL with the LC and QC method for time step $\beta = 2{\cdot}0$

included in order to get insight into the numerical stability and accuracy of the results with respect to different β values. $1{\cdot}0 \leqslant \beta \leqslant 4{\cdot}0$ are selected in the numerical study.

3.1. A bar subjected to uniform ramp-step load

A rectangular bar with left end fixed is subjected to a uniform ramp step load at the other end (see Figure 3). A mesh of 88 nodes and 44 quadratic elements as shown in Figure 3(c) is used. The lateral sides (top and bottom) are assumed to be traction-free. In order to simulate pure 1-D behaviour, the Poisson's ratio of the material is assumed to be zero. This will facilitate a comparison with available analytical 1-D solutions. This problem was also solved numerically by

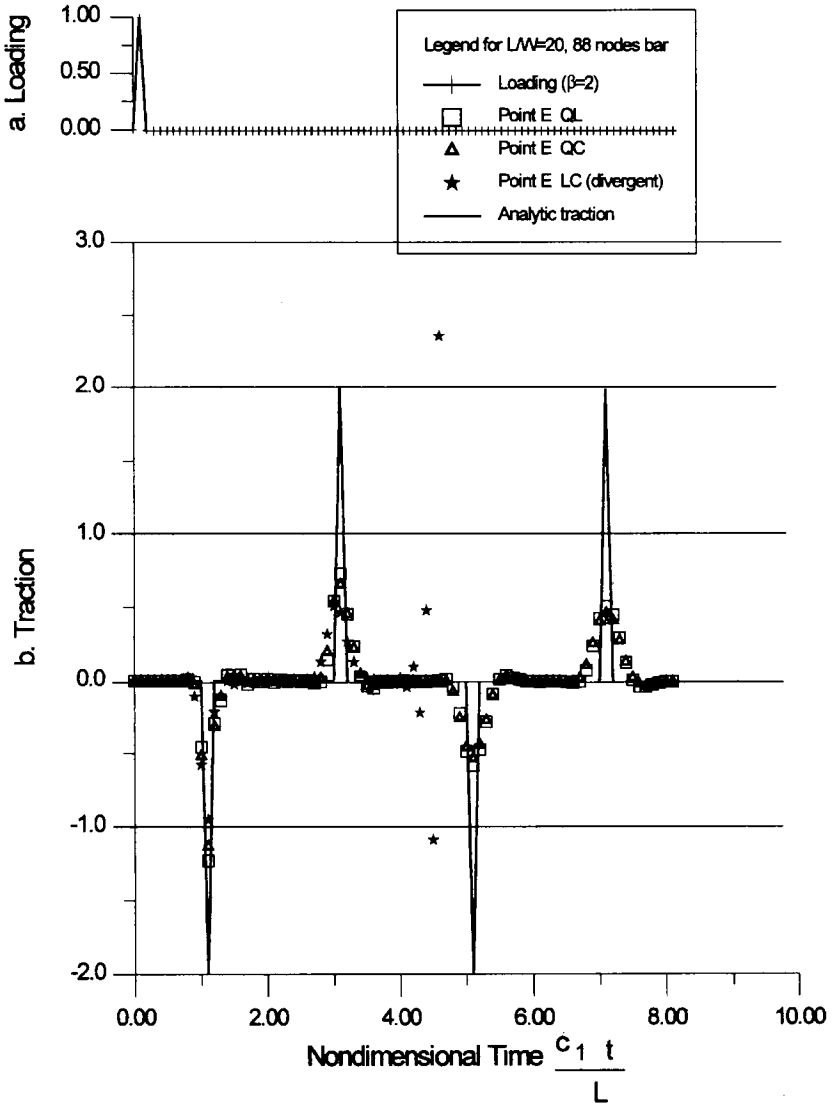

Figure 15. Comparison of the QL with the LC and QC method for time step $\beta = 2{\cdot}0$

many authors to validate their methods. The other material constants are $E = 7{\cdot}8$ Pa and $c_1 = 100\,\mathrm{m\,s^{-1}}$.

Figures 4(b) and 5(b) show the numerical results of displacements at the free end and fixed end tractions of the bar for $\beta = 1{\cdot}0$, respectively. The displacements at point D (see Figure 3(c) for its position) at the free end by all three numerical methods are almost the same as the analytical results as can be seen from Figure 4(b) for $\beta = 1$. But the tractions at point C exhibit a little fluctuation about analytic solution as shown in Figure 5(b) in which QL and LC methods, for a short non-dimensional time, provide a better agreement with the analytical result than QC method does.

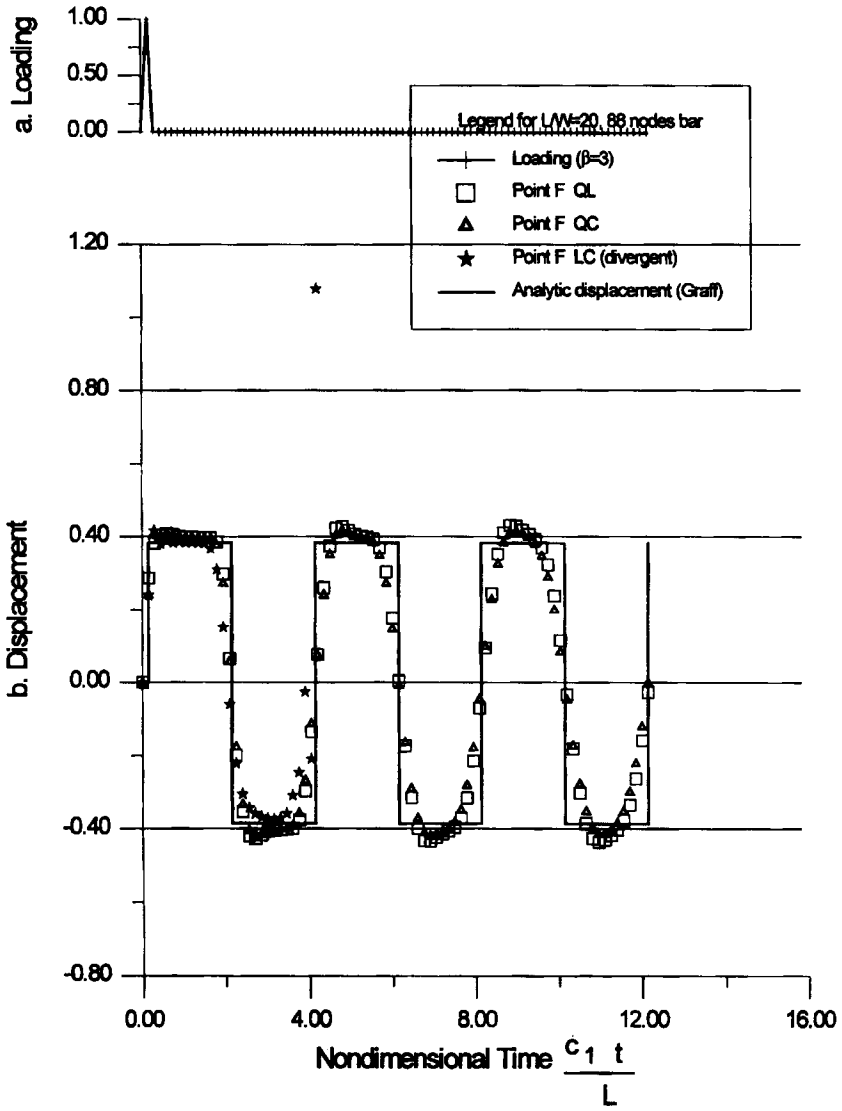

Figure 16. Comparison of the QL with the LC and QC method for time step $\beta = 3{\cdot}0$

For $\beta = 2$, QL and QC methods show good displacement results at point D (see Figure 6(b)) for all 81 time steps, while LC method becomes divergent above $N = 27$. Besides, in the later time steps, QL method gives better traction results at point C than QC method does as shown in Figure 7(b). As seen in Figures 4–11, the accuracy of the numerical results of displacement is always better than that of the results of traction as mentioned in many reports regarding transient problems.

For $\beta = 3$, the LC method leads to divergent results in Figures 8(b) and 9(b) and the results by QL method are closer to analytical solution than those by QC method.

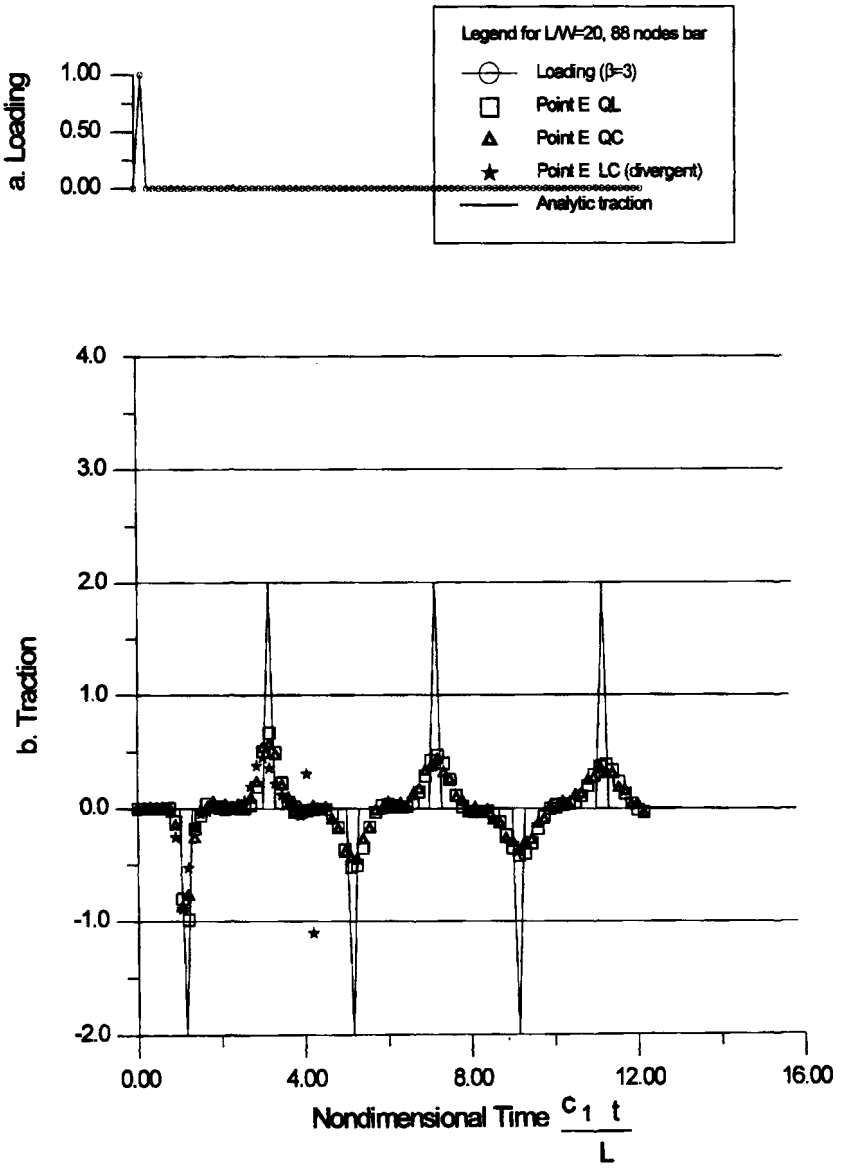

Figure 17. Comparison of the QL with the LC and QC method for time step $\beta = 3{\cdot}0$

For $\beta = 4$, the LC method becomes unstable at a much earlier time than for $\beta = 3$ which is not shown in Figures 10(b) and 11(b). It is seen from those figures that the QL method gives good solutions, while QC method provides oscillating results and becomes divergent at later time. Figures 8(b) and 10(b) show that the displacement amplitude at point D becomes smaller as time increases, which is similiar to a damping effect happened in a viscous system.

Referring to Figures 4–11 and comparing the accuracy and the stability of the QL method with that of the QC method and the LC method for $\beta = 1, 2, 3$ and 4, one can find both the QL method and the QC method are more accurate and stable than that of the LC method as indicated in these figures. The behaviour of the numerical results of Figures 8–11 after a short

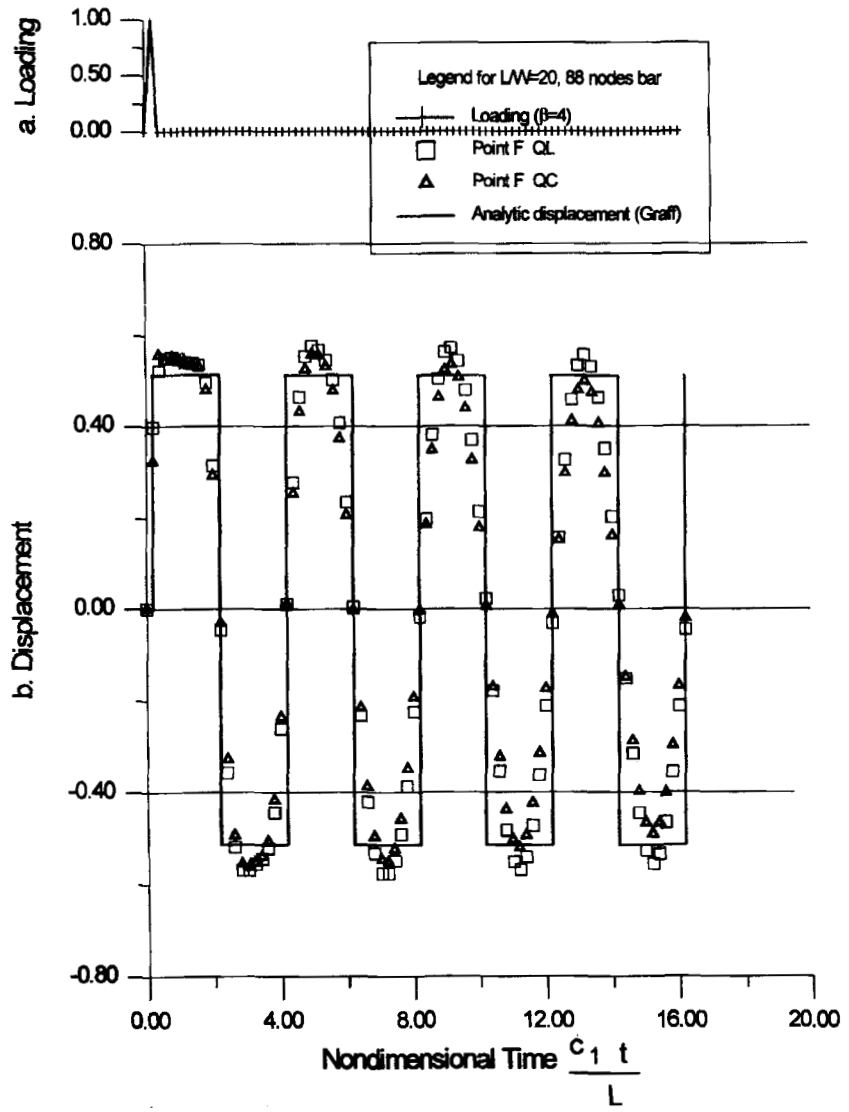

Figure 18. Comparison of the QL with the LC and QC method for time step $\beta = 4{\cdot}0$

non-dimensional time for $\beta \geqslant 2$ reveals that both QL and QC methods approach analytic solution with only a little damping effect, and the LC method gives divergent (unstable) results. In Figures 8–11, the results of LC method are not shown after a small non-dimensional time, since it becomes divergent.

The discrepancy between QL results and analytical solution is smaller than that between QC and analytical solution and this difference reveals that the QL method is more accurate than the QC method.

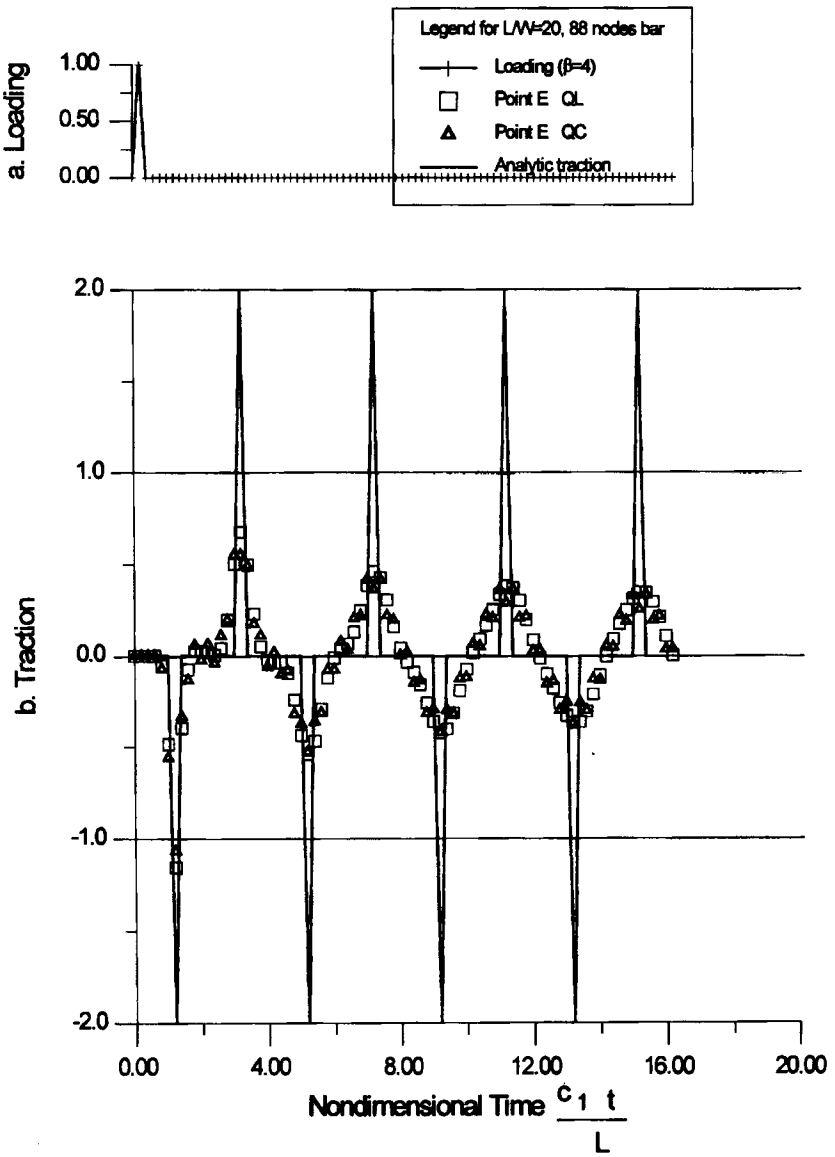

Figure 19. Comparison of the QL with the LC and QC method for time step $\beta = 4{\cdot}0$

3.2. A bar subjected to an impulsive loading

An impulse (Dirac delta) type of load as shown in Figure 12(a) is applied at the right end of a rectangular bar ($L/W = 20$) shown in Figure 3. The lateral sides are still assumed to be traction-free. To simulate pure 1-D behaviour, the Poisson's ratio of the material is assumed to be zero. This will also facilitate a comparison with available analytical solutions. The material constants are $E = 7{\cdot}8$ Pa, $v = 0$ and $c_0 = c_1 = 100\,\mathrm{m\,s^{-1}}$.

The analytical solution[14] for this problem with a loading amplitude P is

$$u(x,t) = \frac{P}{\rho c_0}\left(\left\{H\left[t - \left(\frac{L-x}{c_0}\right)\right] - H\left[t - \left(\frac{L+x}{c_0}\right)\right]\right\}\right.$$

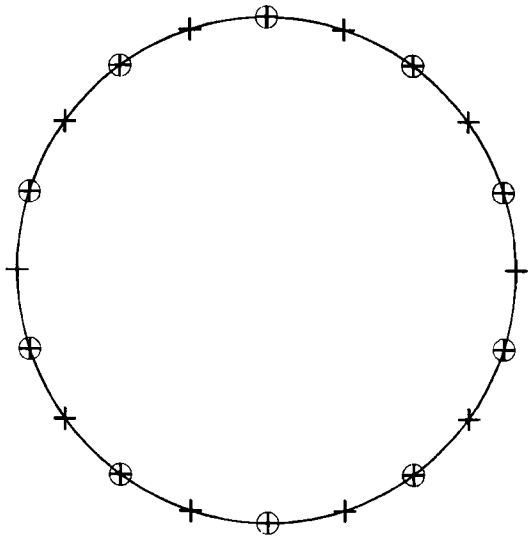

a. 20 nodes, R_0=2

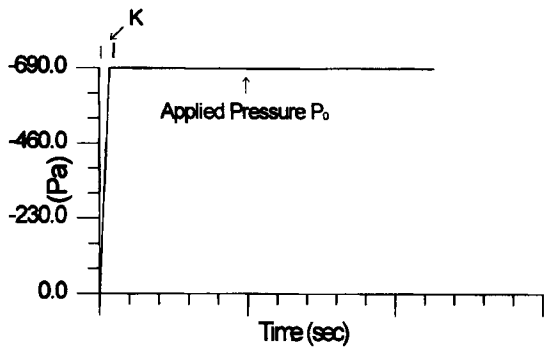

b. Loading curve f(t)

Figure 20. Discretization of the circular cylindrical cavity, (a) 20 nodes, (b) loading curve

$$-\left\{H\left[t-\left(\frac{3L-x}{c_0}\right)\right]-H\left[t-\left(\frac{3L+x}{c_0}\right)\right]\right\}$$
$$+\left\{H\left[t-\left(\frac{5L-x}{c_0}\right)\right]-H\left[t-\left(\frac{5L+x}{c_0}\right)\right]\right\}-\cdots\Bigg) \tag{26}$$

The numerical results by QL, QC and LC methods for the displacement at the free end and the traction at the fixed end are compared with analytical solution for $\beta = 1, 2, 3$ and 4 in Figures 12–19. For $\beta = 1{\cdot}0$, one can see that all three methods give very good results at point F. Surprisingly, the LC method gives more stable traction solutions than QC and QL methods do, but it gives less than half of the analytical value at the second peak where QC and QL methods still give good results.

For larger time step $\beta = 2$, 3 and 4, both QL and QC methods still give fair results, while LC method diverges after a few time steps. But both QL and QC methods are not able to accurately predict the peak of the traction due to such an impulse load with larger time step size.

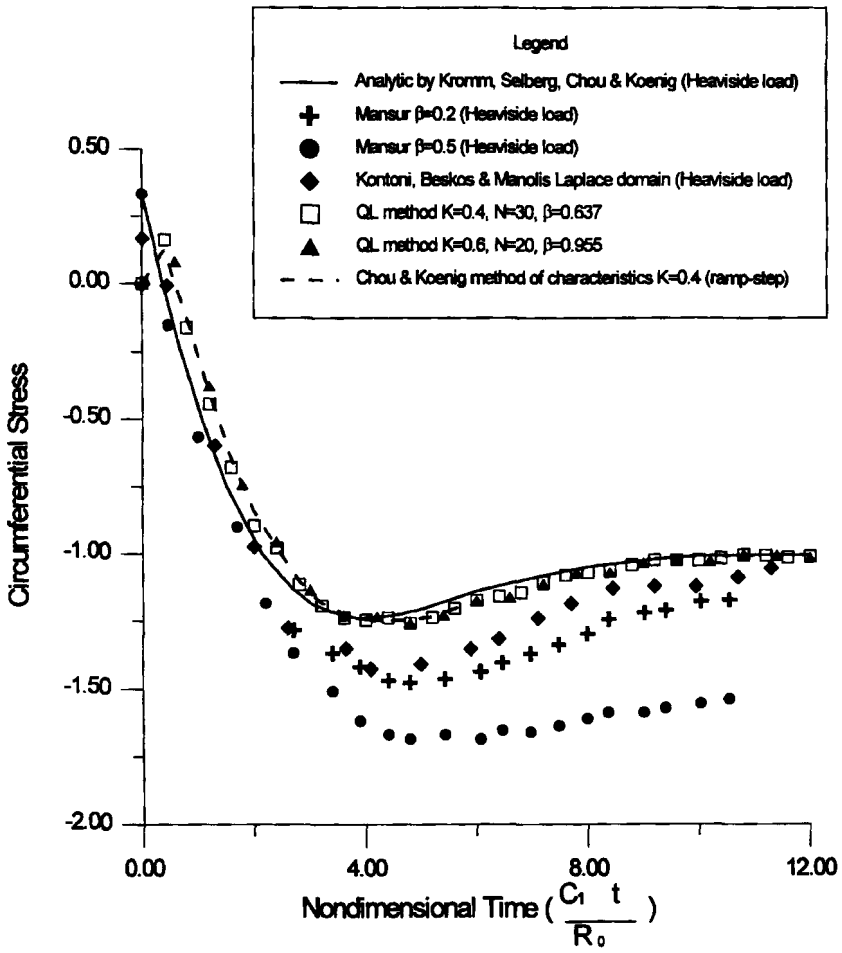

Figure 21. Circumferential stresses at cavity surface due to a ramp-step transient compress wave ($R_0 = 2{\cdot}0$, $\nu = \frac{1}{4}$, plane strain)

3.3. *Transient compression wave from a cylindrical cavity*

Consider a circular cylindrical cavity with radius R_0 in an infinite elastic medium subjected to a suddenly applied internal uniform pressure of intensity P_0. As shown in Figure 20(b) the applied pressure is independent of the angular co-ordinate θ and can be written in the form $P(t) = P_0 f(t)$ with $f(t) = \frac{1}{K} H[t] + (1 - \frac{1}{K}) H[t - K]$ (i.e. ramp-step loading). It was found that it is appropriate to discretize the boundary surface of the cavity into 10 quadratic elements of equal length as shown in Figure 20(a). The numerical input data are $R_0 = 2$ m, $E = 62\,000$ MPa, $\rho = 2670{\cdot}0$ kg m^{-3}, $\nu = 1/4$, $\lambda = \mu = 24\,800$ MPa, corresponding physically to a granite and time span $T = 0{\cdot}00454653$ s, a number of time steps $N = 6$, 12, 18, 20 and 30, and $P_0 = -690$ Pa are selected in the example.

This problem has been solved by Chou and Koenig[15] using the method of characteristics under plane stress conditions, by Fu[16] using the FEM under plane strain conditions, by Kontoni *et al.* using Laplace domain and by Mansur and Brebbia[4] using time-domain BEM under plane stress conditions. The same problem has been solved analytically using Laplace transform method by Kromm[17] under plane stress condition and by Selberg[18,19] under plane strain condition. Note

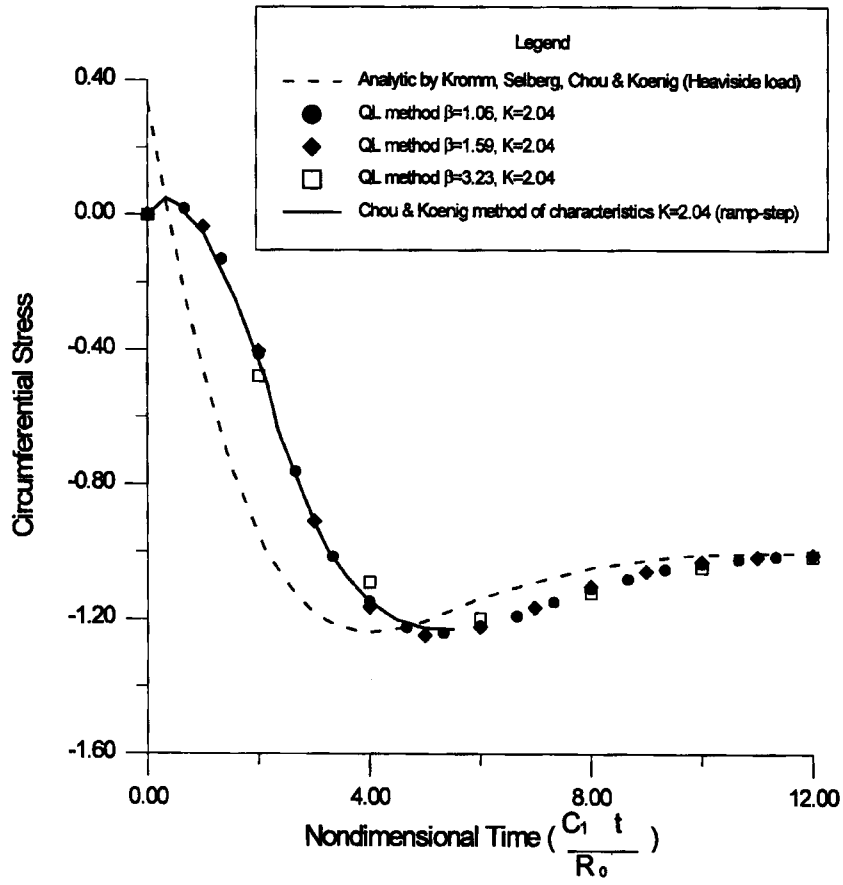

Figure 22. Circumferential stresses at cavity surface due to a ramp-step transient compress wave ($R_0 = 2{\cdot}0$, $\nu = \frac{1}{4}$, plane strain)

that, the plate wave velocity of plane stress, $C_d = (E/\rho(1 - \nu^2))^{1/2}$ and $\nu = \frac{1}{3}$ are adopted as corresponding plane strain case of $\nu = \frac{1}{4}$ for non-dimensional time calculation. Results of Selberg[18] and Kromm[17] agree exactly with those of Chou and Koenig[15].

The time history of the circumferential stress σ_θ at the surface of the cavity by QL method and other methods is plotted in Figure 21. The results by QL method are in very good agreement with analytical solution, except for the first time step. This is due to the difference between Heaviside loading and ramp step loading. Figure 21 reveals that the time history of the circumferential stress at the cavity surface by QL method is in better agreement than that of the Laplace domain and other time-domain methods.

For a ramp-step loading with $K = 2{\cdot}04$, the time history of the circumferential stress σ_θ at the surface of the cavity is plotted in Figure 22 against the method of the characteristic solution.[15] Within plotting accuracy, the results of QL method with $\beta = 1{\cdot}06$ ($N = 18$), $\beta = 1{\cdot}59$ ($N = 12$) and $\beta = 3{\cdot}23$ ($N = 6$) agree exactly with those of Chou and Koenig[15] using ramp input with $K = 2{\cdot}04$.

4. CONCLUSION

After some extensive numerical study of the presented BEM scheme, the following four conclusions can be drawn:

(1) For a ramp-step loading and small time step size, such as $\beta = 1$, all QL, QC and LC methods give good numerical solutions. As time step size increases, for example $\beta \geqslant 2$, LC method goes divergent in a few time steps. The result by the QC method exhibits an oscillating phenomenon and also goes divergent later. But the QL method still gives fair results even for $\beta = 4{\cdot}0$.

(2) For an impulse-type loading, the use of a large time step size should be avoided for all QL, QC and LC methods because of the difficulty in capturing the peak of traction solution, but the QL method can still provide fair results for displacement.

(3) In solving cylindrical cavity problem, the results by QL method agree much better than other numerical solutions with those by analytical methods.

(4) With the same time step size, the QL method (5455·2 s on HP 9000/750) requires about only 31·9 per cent more computing time than that by the LC method (4135·9 s) and 6·6 per cent more than that of the QC method (5116·2 s) for the case with 88 boundary nodes and 81 time steps. And the QL method (308·6 s) needs about only 7·6 per cent more computing time than that by the LC method (286·8 s) and 6·1 per cent more than that of the QC method (290·9 s) for the case with 24 boundary nodes and 61 time steps. However, one should note that the accuracy by the QL method is much better than those by the QC and LC methods. So, it is possible to save computing time by using a larger time step size since a larger β means less computational cost. Restated, the QL and QC methods are capable of saving computational cost and obtaining results much earlier than the LC method, as demonstrated in this present study.

ACKNOWLEDGEMENTS

The authors wish to express their appreciation to the Chung Shan Institute of Science and Technology (CSIST) of Taiwan for the financial support, which makes the research work of the paper possible. The authors would also like to appreciate one of the reviewers for his critical comments which make the paper be written in a better style.

APPENDIX I

Time-convoluted kernels of the QL method

The six combined temporal convolution kernels of the QL method solution procedure, three for displacements and three for tractions, are presented in detail as follows.

Forward linear convoluted displacement kernels of quadratic time step $[G^{N}_{\mathrm{qLF}ij} + G^{N-2}_{\mathrm{qLB}ij}]$ *for N is even* ($N = 2K$).

$$
\begin{aligned}
[G^{2K-1}_{\mathrm{qLF}ij} + G^{2K-2}_{\mathrm{qLB}ij}] = \frac{1}{2\pi\rho}\Bigg\{ & + \left(\frac{\delta_{ij}}{2c_1^2}\right)\Bigg[+ (2K-1)\cosh^{-1}\left\{\frac{c_1(2K-1)\Delta t}{r}\right\} \\
& - 2(2K-2)\cosh^{-1}\left\{\frac{c_1(2K-2)\Delta t}{r}\right\} \\
& + (2K-3)\cosh^{-1}\left\{\frac{c_1(2K-3)\Delta t}{r}\right\}\Bigg] \\
& + \left(\frac{2r_{,i}r_{,j} - \delta_{ij}}{6}\right)\left(\frac{\Delta t}{r}\right)^2\Bigg[+ (2K-1)^2\sqrt{(2K-1)^2 - \left(\frac{r}{c_1\Delta t}\right)^2} \\
& - 2(2K-2)^2\sqrt{(2K-2)^2 - \left(\frac{r}{c_1\Delta t}\right)^2} \\
& + (2K-3)^2\sqrt{(2K-3)^2 - \left(\frac{r}{c_1\Delta t}\right)^2}\Bigg] \\
& - \left(\frac{\delta_{ij} + r_{,i}r_{,j}}{3c_1^2}\right)\Bigg[+ \sqrt{(2K-1)^2 - \left(\frac{r}{c_1\Delta t}\right)^2} \\
& - 2\sqrt{(2K-2)^2 - \left(\frac{r}{c_1\Delta t}\right)^2} + \sqrt{(2K-3)^2 - \left(\frac{r}{c_1\Delta t}\right)^2}\Bigg] \\
& + \left(\frac{\delta_{ij}}{2c_2^2}\right)\Bigg[+ (2K-1)\cosh^{-1}\left\{\frac{c_2(2K-1)\Delta t}{r}\right\} \\
& - 2(2K-2)\cosh^{-1}\left\{\frac{c_2(2K-2)\Delta t}{r}\right\} \\
& + (2K-3)\cosh^{-1}\left\{\frac{c_2(2K-3)\Delta t}{r}\right\}\Bigg] \\
& - \left(\frac{2r_{,i}r_{,j} - \delta_{ij}}{6}\right)\left(\frac{\Delta t}{r}\right)^2\Bigg[+ (2K-1)^2\sqrt{(2K-1)^2 - \left(\frac{r}{c_2\Delta t}\right)^2}
\end{aligned}
$$

$$- 2(2K-2)^2\sqrt{(2K-2)^2-\left(\frac{r}{c_2\Delta t}\right)^2}$$

$$+ (2K-3)^2\sqrt{(2K-3)^2-\left(\frac{r}{c_2\Delta t}\right)^2}\Bigg]$$

$$+\left(\frac{-2\delta_{ij}+r_{,i}r_{,j}}{3c_2^2}\right)\Bigg[+\sqrt{(2K-1)^2-\left(\frac{r}{c_2\Delta t}\right)^2}$$

$$-2\sqrt{(2K-2)^2-\left(\frac{r}{c_2\Delta t}\right)^2}+\sqrt{(2K-3)^2-\left(\frac{r}{c_2\Delta t}\right)^2}\Bigg]\Bigg\} \tag{27}$$

First time step of linear convoluted displacement kernels $[G^N_{\mathrm{iLF}ij}+G^{N-1}_{\mathrm{iLB}ij}]$ *for N is odd* $(N=2K+1)$.

$$[G^{2K+1}_{\mathrm{LF}ij}+G^{2K}_{\mathrm{LB}ij}]=\frac{1}{2\pi\rho}\Bigg\{+\left(\frac{\delta_{ij}}{2c_1^2}\right)\Bigg[+(2K+1)\cosh^{-1}\left\{\frac{c_1(2K+1)\Delta t}{r}\right\}$$

$$-2(2K)\cosh^{-1}\left\{\frac{c_1(2K)\Delta t}{r}\right\}+(2K-1)\cosh^{-1}\left\{\frac{c_1(2K-1)\Delta t}{r}\right\}\Bigg]$$

$$+\left(\frac{2r_{,i}r_{,j}-\delta_{ij}}{6}\right)\left(\frac{\Delta t}{r}\right)^2\Bigg[+(2K+1)^2\sqrt{(2K+1)^2-\left(\frac{r}{c_1\Delta t}\right)^2}$$

$$-2(2K)^2\sqrt{(2K)^2-\left(\frac{r}{c_1\Delta t}\right)^2}+(2K-1)^2\sqrt{(2K-1)^2-\left(\frac{r}{c_1\Delta t}\right)^2}\Bigg]$$

$$-\left(\frac{\delta_{ij}+r_{,i}r_{,j}}{3c_1^2}\right)\Bigg[+\sqrt{(2K+1)^2-\left(\frac{r}{c_1\Delta t}\right)^2}-2\sqrt{(2K)^2-\left(\frac{r}{c_1\Delta t}\right)^2}$$

$$+\sqrt{(2K-1)^2-\left(\frac{r}{c_1\Delta t}\right)^2}\Bigg]$$

$$+\left(\frac{\delta_{ij}}{2c_2^2}\right)\Bigg[+(2K+1)\cosh^{-1}\left\{\frac{c_2(2K+1)\Delta t}{r}\right\}$$

$$-2(2K)\cosh^{-1}\left\{\frac{c_2(2K)\Delta t}{r}\right\}+(2K-1)\cosh^{-1}\left\{\frac{c_2(2K-1)\Delta t}{r}\right\}\Bigg]$$

$$-\left(\frac{2r_{,i}r_{,j}-\delta_{ij}}{6}\right)\left(\frac{\Delta t}{r}\right)^2\Bigg[+(2K+1)^2\sqrt{(2K+1)^2-\left(\frac{r}{c_2\Delta t}\right)^2}$$

$$- 2(2K)^2\sqrt{(2K)^2-\left(\frac{r}{c_2\Delta t}\right)^2}+(2K-1)^2\sqrt{(2K-1)^2-\left(\frac{r}{c_2\Delta t}\right)^2}\Bigg]$$

$$+\left(\frac{-2\delta_{ij}+r_{,i}r_{,j}}{3c_2^2}\right)\Bigg[+\sqrt{(2K+1)^2-\left(\frac{r}{c_2\Delta t}\right)^2}$$

$$-2\sqrt{(2K)^2-\left(\frac{r}{c_2\Delta t}\right)^2}+\sqrt{(2K-1)^2-\left(\frac{r}{c_2\Delta t}\right)^2}\Bigg]\Bigg\} \tag{28}$$

Middle-point linear convoluted displacement kernels of quadratic time step $[G^N_{\mathrm{qLM}ij}] = [G^N_{\mathrm{ILF}ij} + G^{N-1}_{\mathrm{ILB}ij}]$ *for N is even* ($N = 2K$).

$$[G^{2K}_{\mathrm{LF}ij} + G^{2K-1}_{\mathrm{LB}ij}] = \frac{1}{2\pi\rho}\Bigg\{+\left(\frac{\delta_{ij}}{2c_1^2}\right)\Bigg[+(2K)\cosh^{-1}\left\{\frac{c_1(2K)\Delta t}{r}\right\}$$

$$-2(2K-1)\cosh^{-1}\left\{\frac{c_1(2K-1)\Delta t}{r}\right\}$$

$$+(2K-2)\cosh^{-1}\left\{\frac{c_1(2K-2)\Delta t}{r}\right\}\Bigg]$$

$$+\left(\frac{2r_{,i}r_{,j}-\delta_{ij}}{6}\right)\left(\frac{\Delta t}{r}\right)^2\Bigg[+(2K)^2\sqrt{(2K)^2-\left(\frac{r}{c_1\Delta t}\right)^2}$$

$$-2(2K-1)^2\sqrt{(2K-1)^2-\left(\frac{r}{c_1\Delta t}\right)^2}$$

$$+(2K-2)^2\sqrt{(2K-2)^2-\left(\frac{r}{c_1\Delta t}\right)^2}\Bigg]$$

$$-\left(\frac{\delta_{ij}+r_{,i}r_{,j}}{3c_1^2}\right)\Bigg[+\sqrt{(2K)^2-\left(\frac{r}{c_1\Delta t}\right)^2}-2\sqrt{(2K-1)^2-\left(\frac{r}{c_1\Delta t}\right)^2}$$

$$+\sqrt{(2K-2)^2-\left(\frac{r}{c_1\Delta t}\right)^2}\Bigg]$$

$$+\left(\frac{\delta_{ij}}{2c_2^2}\right)\Bigg[+(2K)\cosh^{-1}\left\{\frac{c_2(2K)\Delta t}{r}\right\}$$

$$-2(2K-1)\cosh^{-1}\left\{\frac{c_2(2K-1)\Delta t}{r}\right\}$$

$$+(2K-2)\cosh^{-1}\left\{\frac{c_2(2K-2)\Delta t}{r}\right\}\Bigg]$$

$$-\left(\frac{2r_{,i}r_{,j}-\delta_{ij}}{6}\right)\left(\frac{\Delta t}{r}\right)^2\Bigg[+(2K)^2\sqrt{(2K)^2-\left(\frac{r}{c_2\Delta t}\right)^2}$$

$$-2(2K-1)^2\sqrt{(2K-1)^2-\left(\frac{r}{c_2\Delta t}\right)^2}$$

$$+(2K-2)^2\sqrt{(2K-2)^2-\left(\frac{r}{c_2\Delta t}\right)^2}\Bigg]$$

$$+\left(\frac{-2\delta_{ij}+r_{,i}r_{,j}}{3c_2^2}\right)\Bigg[+\sqrt{(2K)^2-\left(\frac{r}{c_2\Delta t}\right)^2}$$

$$-2\sqrt{(2K-1)^2-\left(\frac{r}{c_2\Delta t}\right)^2}+\sqrt{(2K-2)^2-\left(\frac{r}{c_2\Delta t}\right)^2}\Bigg]\Bigg\} \tag{29}$$

First time step of linear convoluted traction kernels of quadratic time step $[F^{2K+1}_{\mathrm{LF}ij}+F^{2K}_{\mathrm{QB}ij}]$.

$$[F^{2K+1}_{\mathrm{LF}ij}+F^{2K}_{\mathrm{QB}ij}]=\frac{\mu}{2\pi\rho r}\Bigg\{-\left(\frac{A^1_{ij}}{2c_1^2}\right)\Bigg[2\sqrt{(2K+1)^2-\left(\frac{r}{c_1\Delta t}\right)}+(2K-5)\sqrt{(2K)^2-\left(\frac{r}{c_1\Delta t}\right)^2}$$

$$-(2K-1)\sqrt{(2K-2)^2-\left(\frac{r}{c_1\Delta t}\right)^2}\Bigg]$$

$$+\left(\frac{A^2_{ij}}{3}\right)\left(\frac{\Delta t}{r}\right)^2\Bigg[+2(2K+1)^2\sqrt{(2K+1)^2-\left(\frac{r}{c_1\Delta t}\right)^2}$$

$$+(K-5)(2K)^2\sqrt{(2K)^2-\left(\frac{r}{c_1\Delta t}\right)^2}$$

$$-(K)(2K-2)^2\sqrt{(2K-2)^2-\left(\frac{r}{c_1\Delta t}\right)^2}\Bigg]$$

$$+\left(\frac{A^2_{ij}}{6c_1^2}\right)\Bigg[-4\sqrt{(2K+1)^2-\left(\frac{r}{c_1\Delta t}\right)^2}-5(K-2)\sqrt{(2K)^2-\left(\frac{r}{c_1\Delta t}\right)^2}$$

$$+(5K-3)\sqrt{(2K-2)^2-\left(\frac{r}{c_1\Delta t}\right)^2}\Bigg]$$

$$+\left(\frac{2A_{ij}^1+A_{ij}^2}{4c_1^2}\right)\left(\frac{r}{c_1\Delta t}\right)^2\left[+\cosh^{-1}\left(\frac{c_1(2K)\Delta t}{r}\right)\right.$$

$$\left.-\cosh^{-1}\left(\frac{c_1(2K-2)\Delta t}{r}\right)\right]$$

$$+\left(\frac{A_{ij}^3}{2c_2^2}\right)\left[2\sqrt{(2K+1)^2-\left(\frac{r}{c_2\Delta t}\right)^2}+(2K-5)\sqrt{(2K)^2-\left(\frac{r}{c_2\Delta t}\right)^2}\right.$$

$$\left.-(2K-1)\sqrt{(2K-2)^2-\left(\frac{r}{c_2\Delta t}\right)^2}\right]$$

$$-\left(\frac{A_{ij}^2}{3}\right)\left(\frac{\Delta t}{r}\right)^2\left[+2(2K+1)^2\sqrt{(2K+1)^2-\left(\frac{r}{c_2\Delta t}\right)^2}\right.$$

$$+(K-5)(2K)^2\sqrt{(2K)^2-\left(\frac{r}{c_2\Delta t}\right)^2}$$

$$\left.-(K)(2K-2)^2\sqrt{(2K-2)^2-\left(\frac{r}{c_2\Delta t}\right)^2}\right]$$

$$-\left(\frac{A_{ij}^2}{6c_2^2}\right)\left[-4\sqrt{(2K+1)^2-\left(\frac{r}{c_2\Delta t}\right)^2}-5(K-2)\sqrt{(2K)^2-\left(\frac{r}{c_2\Delta t}\right)^2}\right.$$

$$\left.+(5K-3)\sqrt{(2K-2)^2-\left(\frac{r}{c_2\Delta t}\right)^2}\right]$$

$$-\left(\frac{2A_{ij}^3+A_{ij}^2}{4c_2^2}\right)\left(\frac{r}{c_2\Delta t}\right)^2\left[+\cosh^{-1}\left(\frac{c_2(2K)\Delta t}{r}\right)\right.$$

$$\left.\left.-\cosh^{-1}\left(\frac{c_2(2K-2)\Delta t}{r}\right)\right]\right\} \tag{30}$$

Forward quadratic convoluted traction kernels of quadratic time step $[F_{\mathrm{QF}ij}^{2K}+F_{\mathrm{QB}ij}^{2K-2}]$.

$$[F_{\mathrm{QF}ij}^{2K}+F_{\mathrm{QB}ij}^{2K-2}]=\frac{\mu}{2\pi\rho r}\left\{+\left(\frac{2A_{ij}^1+A_{ij}^2}{4c_1^2}\right)\left(\frac{r}{c_1\Delta t}\right)^2\left[\cosh^{-1}\left(\frac{c_1(2K)\Delta t}{r}\right)\right.\right.$$

$$\left.-\cosh^{-1}\left(\frac{c_1(2K-4)\Delta t}{r}\right)\right]$$

$$-\left(\frac{A_{ij}^1}{2c_1^2}\right)\left[(2K-1)\sqrt{(2K)^2-\left(\frac{r}{c_1\Delta t}\right)^2}-6\sqrt{(2K-2)^2-\left(\frac{r}{c_1\Delta t}\right)^2}\right.$$

$$
\begin{aligned}
&- (2K-3)\sqrt{(2K-4)^2 - \left(\frac{r}{c_1\Delta t}\right)^2}\Bigg] \\
&+ \left(\frac{A_{ij}^2}{6c_1^2}\right)\Bigg[- (5K-2)\sqrt{(2K)^2 - \left(\frac{r}{c_1\Delta t}\right)^2} + 12\sqrt{(2K-2)^2 - \left(\frac{r}{c_1\Delta t}\right)^2} \\
&+ (5K-8)\sqrt{(2K-4)^2 - \left(\frac{r}{c_1\Delta t}\right)^2}\Bigg] \\
&+ \left(\frac{A_{ij}^2}{3}\right)\left(\frac{\Delta t}{r}\right)^2\Bigg[(K-1)(2K)^2\sqrt{(2K)^2 - \left(\frac{r}{c_1\Delta t}\right)^2} \\
&- 6(2K-2)^2\sqrt{(2K-2)^2 - \left(\frac{r}{c_1\Delta t}\right)^2} \\
&- (K-1)(2K-4)^2\sqrt{(2K-4)^2 - \left(\frac{r}{c_1\Delta t}\right)^2}\Bigg] \\
&- \left(\frac{2A_{ij}^3 + A_{ij}^2}{4c_2^2}\right)\left(\frac{r}{c_2\Delta t}\right)^2\Bigg[\cosh^{-1}\left(\frac{c_2(2K)\Delta t}{r}\right) - \cosh^{-1}\left(\frac{c_2(2K-4)\Delta t}{r}\right)\Bigg] \\
&+ \left(\frac{A_{ij}^3}{2c_2^2}\right)\Bigg[(2K-1)\sqrt{(2K)^2 - \left(\frac{r}{c_2\Delta t}\right)^2} - 6\sqrt{(2K-2)^2 - \left(\frac{r}{c_2\Delta t}\right)^2} \\
&- (2K-3)\sqrt{(2K-4)^2 - \left(\frac{r}{c_2}\Delta t\right)^2}\Bigg] \\
&- \left(\frac{A_{ij}^2}{6c_2^2}\right)\Bigg[- (5K-2)\sqrt{(2K)^2 - \left(\frac{r}{c_2\Delta t}\right)^2} + 12\sqrt{(2K-2)^2 - \left(\frac{r}{c_2\Delta t}\right)^2} \\
&+ (5K-8)\sqrt{(2K-4)^2 - \left(\frac{r}{c_2\Delta t}\right)^2}\Bigg] \\
&- \left(\frac{A_{ij}^2}{3}\right)\left(\frac{\Delta t}{r}\right)^2\Bigg[(K-1)(2K)^2\sqrt{(2K)^2 - \left(\frac{r}{c_2\Delta t}\right)^2} \\
&- 6(2K-2)^2\sqrt{(2K-2)^2 - \left(\frac{r}{c_2\Delta t}\right)^2} \\
&- (K-1)(2K-4)^2\sqrt{(2K-4)^2 - \left(\frac{r}{c_2\Delta t}\right)^2}\Bigg]\Bigg\} \qquad (31)
\end{aligned}
$$

Middle-point quadratic convoluted traction kernels of quadratic time step $[F^{2K}_{QMij}]$.

$$
\begin{aligned}
[F^{2K}_{QMij}] = \frac{\mu}{2\pi\rho r}\Bigg\{ & -\left(\frac{A^1_{ij}}{c_1^2}\right)\Bigg[-(2K-2)\sqrt{(2K)^2-\left(\frac{r}{c_1\Delta t}\right)^2} + (2K)\sqrt{(2K-2)^2-\left(\frac{r}{c_1\Delta t}\right)^2}\Bigg] \\
& + \left(\frac{2A^2_{ij}}{3}\right)\left(\frac{\Delta t}{r}\right)^2\Bigg[-(K-2)(2K)^2\sqrt{(2K)^2-\left(\frac{r}{c_1\Delta t}\right)^2} \\
& + (K+1)(2K-2)^2\sqrt{(2K-2)^2-\left(\frac{r}{c_1\Delta t}\right)^2}\Bigg] \\
& + \left(\frac{A^2_{ij}}{3c_1^2}\right)\Bigg[+(5K-4)\sqrt{(2K)^2-\left(\frac{r}{c_1\Delta t}\right)^2} - (5K-1)\sqrt{(2K-2)^2-\left(\frac{r}{c_1\Delta t}\right)^2}\Bigg] \\
& + \left(\frac{2A^1_{ij}+A^2_{ij}}{2c_1^2}\right)\left(\frac{r}{c_1\Delta t}\right)^2\Bigg[-\cosh^{-1}\left(\frac{c_1(2K)\Delta t}{r}\right) + \cosh^{-1}\left(\frac{c_1(2K-2)\Delta t}{r}\right)\Bigg] \\
& + \left(\frac{A^3_{ij}}{c_2^2}\right)\Bigg[-(2K-2)\sqrt{(2K)^2-\left(\frac{r}{c_2\Delta t}\right)^2} + (2K)\sqrt{(2K-2)^2-\left(\frac{r}{c_2\Delta t}\right)^2}\Bigg] \\
& - \left(\frac{2A^2_{ij}}{3}\right)\left(\frac{\Delta t}{r}\right)^2\Bigg[-(K-2)(2K)^2\sqrt{(2K)^2-\left(\frac{r}{c_2\Delta t}\right)^2} \\
& + (K+1)(2K-2)^2\sqrt{(2K-2)^2-\left(\frac{r}{c_2\Delta t}\right)^2}\Bigg] \\
& - \left(\frac{A^2_{ij}}{3c_2^2}\right)\Bigg[+(5K-4)\sqrt{(2K)^2-\left(\frac{r}{c_2\Delta t}\right)^2} - (5K-1)\sqrt{(2K-2)^2-\left(\frac{r}{c_2\Delta t}\right)^2}\Bigg] \\
& - \left(\frac{2A^3_{ij}+A^2_{ij}}{2c_2^2}\right)\left(\frac{r}{c_2\Delta t}\right)^2\Bigg[-\cosh^{-1}\left(\frac{c_2(2K)\Delta t}{r}\right) + \cosh^{-1}\left(\frac{c_2(2K-2)\Delta t}{r}\right)\Bigg]\Bigg\}
\end{aligned}
\tag{32}
$$

REFERENCES

1. C. A. Brebbia, J. C. F. Telles and L. C. Wrobel, *Boundary Element Techniques. Theory and Applications in Engineering*, Springer, Berlin, 1984.
2. T. A. Cruse and F. J. Rizzo, 'A direct formulation and numerical solution of the general transient elastodynamic problem I', *J. Math. Anal. Appl.*, **22**, 244–259 (1968).
3. Y. Niwa, T. Fukui, S. Kato and K. Fujiki, 'An application of the integral equation method to two-dimensional elastodynamics', in *Theoretical and Applied Mechanics Proceeding of the 28th Japan International Congress of Theoretical and Applied Mechanics, 1978*, University of Tokyo Press, 1980, pp. 281–290.
4. W. J. Mansur, 'A time-stepping technique to solve wave propagation problems using the boundary element method', *Ph.D. Thesis*, Southampton University, 1983.
5. H. Antes, 'A boundary element procedure for transient wave propagations in two-dimensional isotropic elastic media', *Finite Elements Anal. Des.*, **1**, 313–322 (1985).

6. A. S. M. Israil and P. K. Banerjee, 'Advanced time-domain formulation of BEM for two-dimensional transient elastodynamics', *Int. j. numer. methods eng.*, **29**, 1421–1440 (1990).
7. A. S. M. Israil and P. K. Banerjee, 'Two-dimensional transient wave propagation problems by time-domain BEM', *Int. J. Solids Struct.*, **26**, 851–864 (1990).
8. A. S. M. Israil and P. K. Banerjee, 'Interior stress calculations in 2-D time-domain transient BEM analysis', *Int. J. Solids Struct.*, **27**, 915–927 (1991).
9. C. Wang and H. Takemiya, 'Analytical elements of time domain BEM for two-dimensional scalar wave problems', *Int. j. numer. methods eng.*, **33**, 1737–1754 (1992).
10. C. C. Wang, H. C. Wang and G. S. Liou, 'Quadratic time domain BEM formulation for 2D elastodynamic transient analysis', *Int. J. Solids Struct.*, (1996), to appear.
11. J. H. Kane, *Boundary Element Analysis in Engineering Continuum Mechanics*. Prentice-Hall, Englewood Cliffs, N.J., 1994.
12. C. A. Brebbia and J. Dominguez, *Boundary Elements. An Introductory Course*, Computational Mechanics Publications, Avon, U.K., 1989.
13. A. C. Eringen and E. S. Suhubi, *Elastodynamics*, Vol.II, Academic Press, New York, 1975.
14. K. F. Graff. *Wave Motion in Elastic Solids*, Ohio State University Press, 1975.
15. P. C. Chou and H. A. Koenig, 'A unified approach to cylindrical and spherical elastic waves by method of characteristics', *J. Appl. Mech. ASME*, **33**, 159–167 (1966).
16. C. C. Fu, 'A method for the numerical integration of the equations of motion arising from a finite-element analysis', *J. Appl. Mech. ASME*, **37**, 599–605 (1970).
17. A. Kromm, 'Zur Ausbreitung von Stoßwellen in Kreislochscheiben', *Zeitschrift für angewandte Mathematik und Mechanik*, **28**, 104–114 and 297–303 (1948).
18. H. L. Selberg, 'Transient compression waves from spherical and cylindrical cavities', *Arkiv för fysik*, **5**, 97–108 (1952).
19. J. Miklowitz, *The Theory of Elastic Waves and Waveguides*, North Holland, Amsterdam, 1978.